MR Imaging Surrogate Marker Development in Cross Relaxation Imaging of Cartilage

by

Nade Sritanyaratana

A dissertation submitted in partial fulfillment of

the requirements for the degree of

Doctor of Philosophy

(Biomedical Engineering)

at the

UNIVERSITY OF WISCONSIN-MADISON

2014

Date of final oral examination: 04/25/14

The dissertation is approved by the following members of the Final Oral Committee:
Walter F. Block, Professor, Biomedical Engineering
Richard Kijowski, Associate Professor (CHS), Radiology
Alexey Samsonov, Associate Scientist, Radiology
Darryl Thelen, Professor, Biomedical Engineering
Wan-Ju Li, Assistant Professor, Biomedical Engineering
Oliver Wieben, Associate Professor, Radiology

Abstract

Osteoarthritis is one of the most prevalent chronic diseases in the United States and worldwide. Characteristic changes in the macromolecular matrix of articular cartilage occur during osteoarthritis including a decrease in proteoglycan content and disruption of the highly organized collagen fiber network. Techniques to non-invasively assess the cartilage macromolecular matrix would be beneficial in osteoarthritis research studies to monitor disease-related and treatment-related changes in the composition and ultra-structure of cartilage.

Cross-relaxation imaging (CRI) is a qMT method which can acquire three-dimensional parametric maps of articular cartilage measuring the fraction of macromolecular bound protons (f), the exchange rate constant between macromolecular bound protons and free water protons (k), and the T_2 relaxation time of macromolecular bound protons (T_2^B) with high resolution and relatively short scan time based upon a limited number of MT-contrast images. Modified Cross-Relaxation Imaging (mCRI) is a qMT model closely based from CRI, which corrects for parametric biases due to T_1 mapping. This work utilizes mCRI to model qMT parameters in cartilage.

The goal of this work is to develop non-invasive MRI biomarkers for assessing the content and ultra-structure of the cartilage. This work addresses multiple aspects of biomarker development, including model selection, protocol optimization, clinical feasibility, ex-vivo protocol development, and acceleration techniques for faster acquisitions.

Table of Contents

Summary of Work

Magnetic Resonance Imaging (MRI) is a versatile imaging modality that allows for a wide range of clinical and biological applications. MRI is a major technique for disease diagnosis, and provides excellent soft-tissue contrast without requiring ionizing radiation. Because of the modularity of hardware and software in MR systems and the different possible combinations and settings of pulse sequences in obtaining tissue contrast, MRI applications abound, especially in neurological, cardiac, liver, respiratory, and musculoskeletal contexts.

Conventional qualitative MRI is useful for detecting acute morphological changes in tissue, but quantitative imaging is necessary for detecting intrasubject longitudinal changes (e.g., chronic pain), comparing chronic changes with similar morphological defects, and understanding the biological meaning of MR parameters in tissue. Quantitative imaging promises to provide meaning to each pixel, beyond the collective composition of pixels in an image. For these reasons, quantitative imaging is highly attractive for understanding and eventually diagnosing degenerative joint disease.

Osteoarthritis (OA) is one of the most prevalent chronic diseases in the United States and a significant socioeconomic burden on American society[1]. With an estimated prevalence rate of approximately 20% of the American adult population, OA affects more than 43 million individuals. More than 51 billion dollars is spent annually to treat patients with OA, and the disease limits everyday activities for over 16 million Americans. The current disability and

economic burden associated with OA is enormous. However, the future burden will be considerably higher with the increasing age of the American population [1–5].

Chapter 1 Background provides an introduction of cartilage and MRI applications that frame the motivation for this work. Cartilage biology is first discussed from a macromolecular standpoint. Next is a discussion of osteoarthritis and its implications in healthcare. Different MRI approaches for investigating osteoarthritis are presented, to provide the current state of research in cartilage MRI. The magnetization transfer (MT) phenomenon is introduced, including its usefulness in probing cartilage biology. The chapter culminates into an overview of quantitative MT methods and a more in-depth discussion of one of these methods called cross-relaxation imaging (CRI), which heavily influenced the qMT model used for this work.

Chapter 2 Image Acquisition Development and Model Selection for In Vivo Cross Relaxation Measurement explores the protocol development of a quantitative method to probe cartilage structure and composition. Protocol development heavily depends on the selected quantitative model to provide accurate and meaningful information about cartilage structure and composition. Optimization is also necessary due to the need for successive images to calculate meaningful parametric information and the need for high-resolution imaging in cartilage.

Chapter 3 Cross Relaxation Parameter Study of In-Vivo Human Patellar Cartilage in Two Subject Populations describes in-vivo modified cross relaxation imaging (mCRI) parameters of human patellar cartilage. mCRI parameters in human patellar are measured in-vivo and

compared between healthy volunteers and patients with osteoarthritis. The results of this study provide a strong indication that mCRI parameters are sensitive to changes in degenerative joint disease.

Chapter 4 Methods for Measuring the Stability and Biological Significance of Cross Correlation Parameters using Ex-Vivo Pre-clinical Models presents the development of an mCRI protocol for ex-vivo cartilage applications. Due to the change in tissue environment and the capacity for longer imaging times in an ex-vivo context compared to an in-vivo context, protocol development of mCRI parameters in ex-vivo animal models require changes in imaging settings and post-processing strategies.

Chapter 5 A Compressed Sensing Strategy for Accelerating MSK qMT Applications disseminates the acceleration of qMT imaging in musculoskeletal applications via a Compressed Sensing strategy. This strategy accelerates MT image acquisition in tissue environments rich in fat, due to the sparsity that can be obtained through the subtraction of MT images. The strategy is simulated on digital phantoms to explore possible distortions due to image assumptions and compares this to distortions using conventional acceleration methods. In-vivo data is subsampled to validate the strategy's comparative robustness.

Chapter 6 Summary and Future Work reviews the work disseminated in previous chapters, and suggests the next steps for further understanding cartilage structure and composition in an MRI context.

Chapter 1: Background

1.1 Cartilage Biology

Unlike many tissues, cartilage tissue contains a relatively low number of cells[6]. Chondrocytes make up less than 5% of the cartilage in volume[6]. Despite the low volume, chondrocytes are fundamental to cartilage in that they produce the extracellular matrix (ECM) of the cartilage tissue [7,8], thereby helping to form the cartilage microstructure. The ECM of the cartilage makes up the tissue's main constituent macromolecules and is responsible for cartilage structure and function [6,9]. Changes in the macromolecular content or structure seem to indicate degeneration in the tissue [6,9].

The most prominent macromolecule in the cartilage microstructure is collagen. Type II collagen makes up 15-20% of the wet weight[6,9]. Collagen provides the structural framework for the matrix [6]. The collagen fibers form an intricate structure that can be divided into different layers according to the depth of the cartilage from the articular surface[9].

Another large macromolecular contributor to the wet weight of the cartilage is aggrecan. Aggrecans are large aggregating molecules of proteoglycans (PGs), and make up 3-10% of the weight in articular cartilage[9]. Aggrecan also contains a complex with a protein core with an extended domain that links many glycosaminoglycan (GAG) side chains[9]. In physiologic conditions, the GAGs are densely packed and exhibit a strong negative charge of around as much as 150mM to 300mM in normal articular cartilage[9]. GAG depletion can be used as an early biomarker to detect OA progression[6,9]. In later stages of OA, there is near complete loss of PG [6].

Studies have shown that morphological changes in cartilage succeed irreversible biochemical and structural changes in the tissue[6,9]. One study showed that while there was no visible morphological change in the knee cartilage, physical probing areas of the cartilage with a metallic probe revealed softening of the cartilage[10]. This suggests that conventional morphologic imaging of cartilage would not be sufficient to detect changes due to early OA.

1.1.2 Osteoarthritis

Osteoarthritis is a slow, chronic disease. Early cartilage degradation is characterized by changes in the macromolecular content and microstructure within the cartilage matrix. Metalloproteases, which cleave the cartilage, are first introduced into the cartilage matrix. This progression also involves a decrease in proteoglycan content and disruption of the highly organized collagen fiber network[11–13]. Techniques to non-invasively assess the cartilage macromolecular matrix would be beneficial in osteoarthritis research studies to monitor disease-related and treatment-related changes in the composition and ultra-structure of cartilage[14].

Sensitive methods to detect early cartilage degeneration would also be useful in clinical practice to identify the cause of joint pain in symptomatic patients[15] and to allow early initiation of interventions such as weight loss, aerobic activity, and range of motion and strengthening exercises which may alleviate symptoms and potentially slow the rate of joint degeneration[16(p20)].

1.2 Cartilage MR Imaging

Due to the need for non-invasive methods to accurately track cartilage progression and diagnose osteoarthritis, cartilage MRI has been a widely researched topic and several techniques have been developed to address various aspects of cartilage. Various quantitative magnetic resonance (MR) techniques have been used to evaluate the composition and ultra-structure of articular cartilage. These techniques include delayed gadolinium enhanced spin-lattice relaxation time (T_1) imaging[17,18], sodium imaging[19,20], and spin-lattice relaxation time in the rotating frame (T_{1rho}) imaging[21,22] which are sensitive to changes in the proteoglycan content of degenerative cartilage. In addition, spin-spin relaxation time (T_2) imaging has been used to identify alterations in the macromolecular and water content and disruption of the collagen fiber network associated with cartilage degeneration[23,24]. Diffusion imaging has also been used to detect changes in articular cartilage at various stages of degeneration with the apparent diffusion coefficient assessing changes in water permeability[25,26] and the fractional anisotropy assessing changes in the three-dimensional ultra-structure of the macromolecular matrix[27].

Quantitative MR techniques which investigate magnetization exchange between macromolecular bound protons and free water protons including magnetization transfer ratio (MTR)[28,29] and chemical exchange-dependent saturation transfer (CEST) imaging[30,31] have also been used to evaluate articular cartilage. These techniques utilize the magnetization transfer (MT) effect to acquire information regarding protons bound to the macromolecular matrix of cartilage which cannot be directly assessed using conventional MR methods. Quantitative magnetization transfer

(qMT) imaging is another approach which utilizes a two-pool model of magnetization exchange to acquire information regarding macromolecular bound protons within cartilage[32–34]. However, qMT imaging techniques typically require multiple MT-contrast images with different magnetization preparatory pulses resulting in long scan times which have limited cartilage assessment to ex-vivo specimens[35–37].

A sampling of various cartilage MR techniques is further described below.

dGEMRIC

A variety of non-MT sequences are being investigated for their efficacy in detecting articular cartilage degradation. One particularly successful endeavor involves the use of gadolinium-enhanced contrast agent to illuminate changes in water retention[6,9]. $Gd(DTPA)^{2-}$ is injected into the cartilage tissue, and accumulates in areas with low GAG content[9]. This accumulation can be detected through T_1 mapping[9]. This technique, called dGEMRIC, is an indirect method for measuring GAG content in tissue cartilage[9]. In effect, it is useful for detecting early stage OA[9]. However, T_1 can also be influenced by changes in water content and the permeability of the tissue, confounding the accuracy of GAG detection[9]. Additionally, as with all gadolinium-based contrast agents, care must be taken into the dosage amount for risk of nephrogenic systemic fibrosis, a debilitating condition[9].

Sodium Imaging

In theory, MRI can obtain signal from any molecule with some nonzero charge. It has been demonstrated that due to the high negative charge of the cartilage, there is enough sodium to provide high signal intensity in cartilage imaging with MRI[6,9]. Sodium imaging has been found to provide high specificity for PG content, and provides high contrast without the use of an exogenous contrast agent[9]. However, sodium imaging also requires long imaging times[9]. Sodium imaging also requires the use of specialized coils and high field scanners[9]. Lastly, since this technique requires that the RF pulse excite sodium at its specific resonant frequency, commercial systems limit researchers to use a wide band RF system that would have the ability to produce the correct resonant frequency.

$T_{1\rho}$ Imaging

Quantitative imaging of $T_{1\rho}$ can be used to observe the physiochemical interactions within the macromolecular environment. Frequently used in NMR, $T_{1\rho}$ is the spin-lattice relaxation constant in the rotating field. Due to its high dynamic range, $T_{1\rho}$ imaging is readily sensitive to changes in PG depletion[9]. Thus, $T_{1\rho}$ provides sensitive detection of early cartilage degeneration without the use of exogenous contrast agent[9]. However, $T_{1\rho}$ imaging requires high RF power, which could result in tissue heating and damage due to the specific absorption rate of the tissues[9].

mcDESPOT

Multi-component mcDESPOT may provide information regarding the proteoglycan content of cartilage. Proteoglycan loss within cartilage occurs during the early stages of OA and gradually

increases as the disease progresses[11,12,38]. Previous multi-component T_2 mapping studies using NMR spectroscopy have found that the fraction of the W_{PG} component (F_{PG}) is a sensitive and specific measure of the proteoglycan content of cartilage[39–41].

mcDESPOT may also provide information regarding the integrity of the collagen fiber network of cartilage. While the collagen content of cartilage decreases by only 5% in the advanced stages of OA, disruption of the collagen fiber network is an important initiating event in the disease process[12,13,42–45]. mcDESPOT can measure single-component T_2 relaxation time ($T2_{single}$), which is one of the few MR parameters currently available that provides information regarding collagen fiber orientation and the integrity of the collagen fiber network of cartilage through the magic angle effect[46–51].

1.3 Magnetization Transfer

Principles of Magnetization Transfer

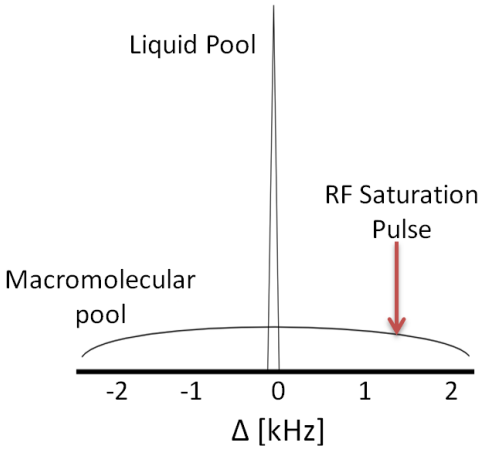

Figure 1-1. Lineshape of tissue depicting classical magnetization transfer[52]. Notice that the water signal provides more signal within a narrower frequency band.

Magnetization transfer is a phenomenon that was accidently discovered by trying to perform a spin transfer experiment by selective saturation of urea looking for small signal suppression in water. Instead, investigators found a significant loss of signal, which did not correspond to the expected loss dependent on the specific offset frequency of the irradiation[52,53].

Conventional MRI derives its signal from mobile water protons that all resonate around some center frequency depending on the gyromagnetic ratio and the field strength of the magnet. Usually, an RF excitation is applied at this on-resonance frequency in order to excite the protons as an imaging source. However, when an off-resonance pulse is applied to tissue before exciting

mobile protons (See **Figure 1-1**), the water pool saturates due to macromolecular content, and lower signal is observed compared to the case without the off-resonance pulse[52]. This contrast effect due to macromolecular content is called the magnetization transfer (MT) effect.

Quantitative MT imaging involves the characterization of the discussed macromolecular lineshape by observing multiple MT measurements taken at different offset frequencies and RF powers[34,54,55]. By increasing the RF power, we observe increased contrast due to macromolecular content (higher MT effect). By increasing the offset frequency, we excite further down the macromolecular lineshape, and thus observe decreased contrast (lower MT effect).

1.3.1 Quantitative Magnetization Transfer

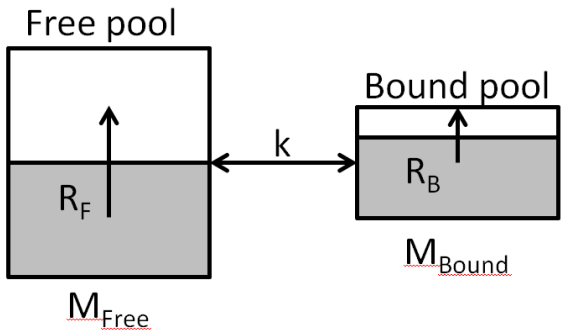

Figure 1-2. Two-Pool Magnetization Transfer Model[52]. Quantitative Magnetization Transfer can be described through this two-pool model.

Quantitative MT can be further described through a model detailing the exchange between the macromolecular and water pools[52]. The macromolecular and water pools quantify the amount of macromolecular and water spins, respectively[52]. This "two-pool model" (See Figure 1-2) also quantifies the exchange between the two pools with exchange rate R[52]. The two shaded regions

describe the saturated spins in each pool, where the saturated spins relax to the unsaturated spins with constants R_A and R_B [52].

Perhaps due to considerations for hardware, protocol design, and mathematical complexity, many different quantitative models have arisen for expressing this two-pool relationship [32,34,54,56–61]. A small subset of these models is described below.

Minimal Approximation Magnetization Transfer (MAMT)[61] solves qMT parameters directly from modified Bloch equations by using the two-pool relationship and modelling RF pulses with a train of rectangular pulses windowed by the shape of the RF pulse. MAMT claims to minimize the approximations required to compute the qMT parameters.

Sled and Pike (2001)[58] introduced a quantitative model capable of obtaining all observable parameters for the two pool model. Using $B_0/B_1/T_1$ mapping and 60 MT-weighted images, they demonstrated that this technique can obtain k_f, F, R_1^f, R_1^r, T_2^f, T_2^r, R_1^{obs}, and T_2^{obs}.

Cross-Relaxation Imaging (CRI)[34,54] is a time efficient method to obtain f and k maps in vivo. CRI can obtain 3D whole brain k and f maps in with 1.4 mm^3 isotropic resolution. CRI samples the bound pool by acquiring multiple MT-weighted images at different offset frequencies with complementary T_1 information.

1.3.2 Cross Relaxation Imaging [34]

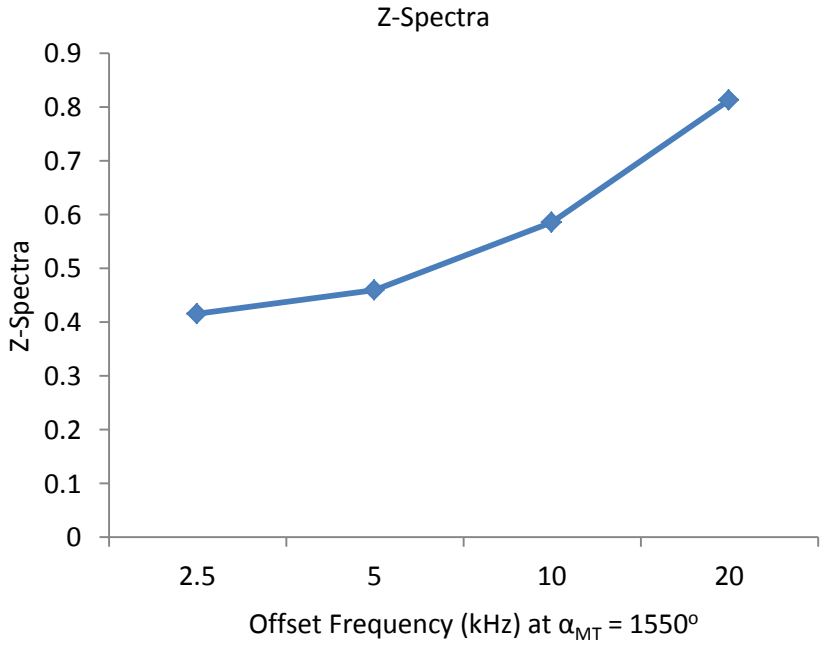

Figure 1-3. Example of z-spectra for knee cartilage. Notice the monotonic increase in the z-spectra with increasing offset frequency. The z-spectra signal is inversely proportional to the amount of saturation from an offset frequency MT excitation. More specifically, z is calculated as the ratio between signal with MT effect and without MT effect. MT signals with low offset frequencies have more saturation, exhibited by a decrease in signal, and therefore a lower z than MT signals excited at higher offset frequencies.

Originally used in analyzing brain tissue pathology, Cross Relaxation Imaging (CRI) uses an array of MT-prepared SPGR images that sample the so-called "z-spectra". The MT reconstruction relies on a number of tightly coupled equations. We first assume that the

absorption line shape of the bound spins is either "super Lorentzian" or "Gaussian", depending on the macromolecule in question. The super Lorentzian line shape $g(\Delta, T_2^B)$, usually used for soft tissues, can be described as:

$$g(\Delta, T_2^B) = \sqrt{\frac{2}{\pi}} \int_0^{\pi/2} \frac{T_2^B}{|2cos^2\theta - 1|} \exp\left(-2\left(\frac{2\pi\Delta T_2^B}{3cos^2\theta - 1}\right)^2\right) sin\theta \, d\theta$$

where Δ is the position of the line shape (aka offset frequency, in Hz) and T_2^B is the macromolecular bound T_2 which parameterizes the width and height of the line shape. To simplify the fitting routine, it is possible to approximate the RF pulse as an effective rectangular pulse B_{1e} as:

$$B_{1e} = \left(\int_0^{t_m} B_1^2(t)dt/t_m\right)^{1/2}$$

The magnetization ratio (MTR), which intuitively is the ratio between the saturated MT signal (M_s) and the unsaturated "zero-offset" signal (M_0), can be easily calculated and used to fit parameters P and Q:

$$MTR = 1 - \frac{M_s(W^B)}{M_0} \approx \frac{sW^B}{P + QsW^B}$$

where $s=t_m/TR$ (t_m being the duration of the MT saturation pulse), and W^B is the average saturation rate for the bound pool described by:

$$W^B = \pi\gamma^2 {B_{1e}}^2 g(\Delta, T_2^B)$$

Finally, parameters P and Q are independent of the RF field saturation and instead dependent on T_2^B, exchange rate constant k, and bound pool fraction f, where the (simplified) relation is described as:

$$P \approx \frac{\left(\frac{1}{T_1^{obs}} - (1-f)(\ln cos\alpha)/TR\right)}{f}$$

$$Q \approx \frac{\left(\frac{1}{T_1^{obs}} - (\ln cos\alpha)/TR\right)}{k} + 1$$

Where f is the bound pool fraction, and k is the exchange rate constant, both physiologically relevant parameters for the given qMT sequence. With two equations and two unknown variables of interest, P and Q provide a unique (linear) solution for f and k. However, if we do not assume a value of T_{2b}, then the problem becomes nonlinear. The MT-weighted images were processed using a pixel-by-pixel nonlinear least-square fitting routine, to fit P, Q, and T_{2b} according to the MTR measurements. P and Q were then used to calculate f and k, respectively.

For cross-relaxation imaging, the characterization of the macromolecular lineshape can be described by 3 unknown parameters. The first parameter is known as the bound pool fraction (f)[34]. Bound pool fraction describes the fraction of macromolecular spins compared to the total spins between the two pools. The second parameter is known as the effective cross-relaxation rate constant (k)[34]. This parameter describes the rate at which the macromolecular pool and the water pool exchange spins. Lastly, the third parameter is known as the bound transverse relaxation constant (T_{2b})[34].

Due to the nature of the CRI model, CRI requires knowledge of other quantitative measures, specifically the B_1 and T_1 of each voxel in the field of view. Typically for CRI applications, B_1 is

acquired through Actual Flip Angle Imaging (AFI), and T_1 is acquired using the Variable Flip Angle (VFA) method (also known as DESPOT1).

B_1 Mapping: Actual Flip Angle Imaging (AFI)[62]

Because the actual RF excitation of each voxel in the knee may vary, it is imperative for CRI that the B_1 is mapped at each pixel. Although the technique could be applied to many biological tissues, AFI was originally used for whole body and brain imaging. The AFI sequence consists of two identical RF pulses each followed by a delay TR. Both delays last different durations ($TR_1<TR_2$). During each of the delays a gradient-echo (GRE) signal is acquired, resulting in two images of different B_1 weighted intensities. Assuming that the repetition times are short and the transverse magnetization is spoiled ($M_{xy} \sim 0$), the ratio of the signal intensities ($r = S_2/S_1$) can be approximated by the first order as a function between the TR ratio ($n = TR_2/TR_1$) and the flip angle (α). More specifically,

$$r = \frac{1 + n\,cos\alpha}{n + cos\alpha}$$

Solving for α, this becomes:

$$\alpha = \cos^{-1}\frac{rn - 1}{n - r}$$

Since B_1 inhomogeneities affect the relative signals of each voxel, accurate T_1 and qMT fitting require B_1 maps to correct the raw images for both fits.

T_1 mapping: Variable Flip Angle (VFA) Imaging [63]

Quantitatively describing the macromolecular pool lineshape requires knowledge of the T_1 of the tissue. In order to map T_1 relaxation times, CRI utilizes a VFA sequence (also known as DESPOT1). VFA imaging was originally used to image the T_1 of brain tissue, although the sequence is not a tissue-specific technique. VFA imaging uses a spoiled gradient echo (SPGR) sequence, which generates a signal intensity (S_{SPGR}) that can be described as a function of T_1, TR, α, and the equilibrium longitudinal magnetization M_0:

$$S_{SPGR} = \frac{M_0(1 - E_1)sin\alpha}{1 - E_1 cos\alpha}$$

where $E_1 = e^{-TR/T_1}$. By taking multiple SPGR acquisitions at different flip angles α, it is possible to generate a curve characterized by T_1. The acquired data can then be linearized to a form Y=mx+b:

$$\frac{S_{SPGR}}{sin\alpha} = E_1 \frac{S_{SPGR}}{tan\alpha} + M_0(1 - E_1)$$

the slope m and the intercept b are estimated by drawing a best fit line using linear regression. m and b are used to extract T_1 and M_0 by a simple relation:

$$T_1 = -TR/\ln(m)$$

$$M_0 = b/(1 - m)$$

R_1 is simply the multiplicative inverse of T_1.

Chapter 2: Model Selection and Image Acquisition Development for In Vivo Cross Relaxation Measurement

This chapter serves to describe the methods used to develop an mCRI protocol for evaluating human patellar cartilage in-vivo at 3.0T which can provide robust measurements of f, k, and T_2^B in a 19 minute scan time.

Additionally, despite the relative advantage of providing fast, robust 3D imaging of qMT parameters compared to other qMT methods, mCRI still demands careful protocol development because the need for multiple magnetization transfer (MT) acquisitions uses valuable scan time. In previous cartilage studies, qMT protocols sampled a wide range of offset frequencies and/or flip angles which resulted in long acquisition times and limited anatomic joint coverage[54,55,64]. One way to decrease scan time is to optimize the selection of these MT combinations to capture similar information with fewer acquisitions. This work proposes and employs a smart search algorithm to intelligently select an appropriate MT combination.

2.1 Introduction

The careful selection of a model for quantifying MT parameters is critical in improving parametric accuracy while providing more meaningful values. Many of these models suffer from long examination time, insufficient anatomic coverage, low quality of parametric maps, and large slice thickness[54]. Cross Relaxation Imaging (CRI) allows for time-efficient image acquisition of MT-prepared images to quantify the two-pool model. However, VFA has been

found to inaccurately describe the SPGR signal in tissues with rich macromolecular content, leading to biased R_1 estimation. In tissues with rich macromolecular content, VFA does not account for the MT effect between macromolecular and water protons, and in these tissues the longitudinal relaxation of water proton magnetization exhibits a biexponential behavior[65]. Thus, since CRI depends on VFA to calculate the two-pool qMT parameters f, k, and T_2^B, calculating these parameters using CRI in tissues with rich macromolecular content will yield biased values.

A modified model, aptly called modified Cross Relaxation Imaging (mCRI)[56], proposes the unified treatment of VFA and MT SPGR signals, enabling the simultaneous correction of R1 and two-pool MT model parameters without the need for additional scans. The previous study provided strong evidence that this unified treatment significantly corrects the biases in neural tissue, which is rich in macromolecular content. This work utilizes mCRI to model qMT parameters in cartilage.

Furthermore, careful protocol development for qMT imaging is necessary because protocols utilize multiple magnetization transfer (MT) acquisitions with different combinations of offset frequencies and flip angles. In previous cartilage studies, qMT protocols sampled a wide range of offset frequencies and/or flip angles which resulted in long acquisition times and limited anatomic joint coverage [54,55,64]. One way to decrease scan time is to optimize selection of these MT combinations in order to create a qMT protocol that can capture similar information with fewer acquisitions. The non-linear nature of the model makes it difficult to intuitively select optimal MT “points”. Searching through combinations consisting of k points in an N point

search space, when using a brute force method, requires $\binom{N}{k} = \frac{N!}{k!(N-k)!}$ calculations for a time complexity $O(N\ choose\ k)$. Large N and small k can result in inordinately long search times. In this study, I propose and employ a smart search algorithm that has time complexity $O(kN)$ to intelligently select an appropriate MT combination.

I performed digital simulations to quantitatively choose the best MT combinations out of an array of offset frequencies and flip angles, and then determine an 8 "point" and a 4 "point" protocol that provide the most precision and accuracy in qMT parameters. Additionally, I used these protocols to provide greater lateral coverage of the in-vivo weight-bearing surfaces of the tibiofemoral joint.

2.2 Theory

Modified Cross Relaxation Imaging (mCRI)[56]

As derived from a previous study[54], the longitudinal magnetization with no off-resonance saturation can be described as

$$M_z = (I - EC)^{-1}(I - E)M_{eq}$$

Where $M_z = \begin{bmatrix} M_z^F \\ M_z^B \end{bmatrix}$corresponds to the longitudinal magnetization before the RF pulse, $M_{eq} = M_0 \begin{bmatrix} 1-f \\ f \end{bmatrix}$ corresponds to the equilibrium magnetization, $E = e^{R*TR}$ corresponds to the relaxation during the repetition time TR, and $C = \begin{bmatrix} \cos\alpha & 0 \\ 0 & 1 \end{bmatrix}$ corresponds to the instant rotation

of the longitudinal magnetization of the free pool. R is the relaxation matrix which can be described by

$$R = \begin{bmatrix} -R_1^F - k & k\dfrac{1-f}{f} \\ k & -R_1^B - k\dfrac{1-f}{f} \end{bmatrix}$$

Where R_1^F and R_1^B are the longitudinal relaxation rates for the free and bound pool, respectively. The longitudinal equation at the top of this section can be simplified through a first order approximation, and its corresponding expression for observed signal can be described as

$$S \approx \frac{M_0(1-f)\left(R_1^F R_1^B + \dfrac{R_1^F k(1-f)}{f} + R_1^B k\right)(\sin\alpha)e^{(-T_E/T_2^*)}}{R_1^F R_1^B + \dfrac{R_1^F k(1-f)}{f} + R_1^B + k - (R_1^B + k(1-f)/f)T_R^{-1} ln(\cos\alpha)}$$

Earlier studies[34,66] assume that $R_1^F = R_1^B = R_1$ due to fast exchange conditions [67], and $R_1 \ll k/f$, so this signal equation simplifies to

$$S \approx M_0(1-f)\frac{R_1 T_R}{R_1 T_R - (1-f)\ln(\cos\alpha)}(\sin\alpha)e^{(-T_E/T_2^*)}$$

As mentioned earlier, compared to Cross-Relaxation Imaging, mCRI corrects for biases in R_1, and without this correction, the apparent R_1 can be described as

$$R_1^{app} \approx \frac{R_1}{(1-f)}$$

For a more thorough treatment of the mCRI model, including its derivation, validation, and comparison to CRI, see Mossahebi et. al.[56].

MT Point Selection Optimization

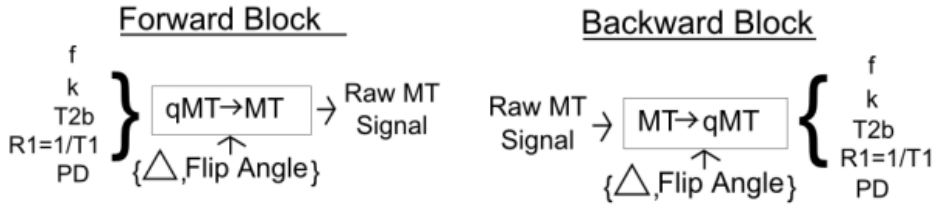

Figure 2-1. The above schemes are essential in conducting a brute force Monte Carlo qMT optimization routine. The forward block is utilized to digitally create raw MT signals for different MT offsets (Δ) and flip angles. Varying noise can be added, and the backward block can be used to measure parameter-to-noise (PNR). The end goal is to maximize the PNR with an optimal set of MT offsets and flip angles.

Digital simulations:

Digital simulations (See **Figure 2-1**) can be performed to determine an optimal qMT protocol for typical qMT values of articular cartilage. The qMT cross-relaxation model as proposed by Yarnkykh[34,54] and later modified by Mossahebi[56] can be solved numerically in the forward direction (Figure 1) using qMT parameters (f, k, T_{2b}), and other tissue parameters (proton density and $R_1=1/T_1$) to obtain raw MT signals of desired MT flip angles and offset frequencies (Δ). qMT parameters can also be solved iteratively in the backward direction (Figure 1), using a non-linear least squares algorithm. To obtain preliminary information about qMT values, we measured qMT parameters (f=12.5%, k=5.4, and T_{2b}=6.56μs) of patellar cartilage in 10 volunteers using a previous 8 point protocol[68], hereby named *Protocol 1*, at different MT offset frequencies and flip angles: 800Hz/1550°, 2.5kHz/1550°, 5kHz/1550°, 10kHz/1550°,

20kHz/1550°, 800Hz/890°, 2.5kHz/890°, 5kHz/890°. Based on these mean qMT values, raw MT signals of desired MT offsets and flip angles were calculated in the forward direction. Normally distributed noise was then added to the raw signals for an SNR of 75 in the MT "off" signal. The signals were then fit in the backward direction to obtain simulated human knee qMT values (f_{sim}, k_{sim}, T_{2b_sim}). A measure of parameter-to-noise ratio was calculated: $PNR_{param} = \frac{median(param_{sim})}{SD(param_{sim})}$, $param: \{f, k, T_{2b}\}$.

Optimization Strategy

The process of optimizing a qMT protocol using Monte Carlo simulations can be designed to be statistically robust. However, searching the entire MT space of different MT offset frequencies and flip angles is computationally intensive: even with just 20 MT offset frequencies and 20 MT flip angles, this results in a 400 MT point search space. Searching all possible 8 MT point combinations requires searching over $\binom{400}{8} \approx 1.515 \times 10^{16}$ combinations. Even if evaluating each combination takes one second, this search would require nearly half a billion years. A smarter search algorithm is required to utilize Monte Carlo simulations for determining an optimal MT point combination.

I designed an iterative voting strategy to efficiently explore the MT space. Using the same above example of searching a 400 MT point space (20 MT offset frequencies and 20 MT flip angles), this voting strategy can be described in a scheme similar to Ives [69]:

1. 399 MT points are fitted to measure the PNR for each parameter (as described above).

2. The sum of PNR is calculated for this 399 MT point combination.
3. The next combination of 399 MT points is chosen and steps 1-2 are repeated to calculate the sum of PNRs. There are 400 possible combinations of 399 MT points (each combination removes one MT point from the 400 MT point search space).
4. Instead of calculating the sum of PNRs for all 400 possible combinations, it is sufficient to consider only 20 combinations—each combination "votes off" an MT point, and we seek only to remove the "worst" MT point seen so far. This worst MT point seen so far is selected by the combination that has the highest sum of PNRs.
5. Voting off the worst MT point results in a 399 MT point combination, which is used to select the best 398 MT point combination (by repeating steps 1-4).
6. Stop when a 20 MT point combination has been selected.

This voting strategy requires evaluating 7600 MT combinations, and if evaluating each combination takes one second, this search would require approximately 2 hours.

The lightweight nature of this voting strategy enables several key benefits:

1. The ability to more finely sample the MT search space (more MT offset frequencies or MT flip angles) to minimize the possibility of falling into local minima.
2. The ability to run multiple simulations to obtain multiple 20 MT point candidates.
3. The ability to combine multiple simulation results and cascade them in a more rigorous Monte Carlo simulation.
4. The ability to combine this strategy with more exhaustive searches while maintaining an acceptable computation time.

In light of these benefits, my implementation of this voting strategy involved the following:

1. Finely sampling the MT search space to 880 unique MT points,
2. Running 3 multiple simulations to obtain 60 MT point candidates,
3. Cascading these 60 MT point candidates to find the best 20 point combination, and
4. Exhaustively searching these 20 MT point candidates to obtain the best 8 MT point combination and the best 4 MT point combination.

2.3 Methods

The optimization strategy as described above was performed using the following:

1. An MT search space of 880 unique MT points: offset frequencies from 2 to 20kHz (in 500Hz increments) and flip angles from 500° to 1550° (in 50^{o} increments), to search for 20 MT point candidates per simulation.
2. 3 repeated simulations to obtain 60 MT point candidates.
3. A cascade optimization using these 60 MT points in a more rigorous Monte Carlo simulation (5X Monte Carlo samples per combination) to find the best 20 MT point combination.
4. All possible 8 MT point and 4 MT point combinations were exhaustively searched in a brute force fashion in the 20 MT point search space.

Based on this strategy, 8 MT points that maximized the sum of PNRs were selected: 2kHz/1550°, 20kHz/1550°, 17kHz/1450°, 18kHz/1350°, 2kHz/750°, 5kHz/750°, 4kHz/700°,

2kHz/600°, hereby referred to as *Protocol 2*. The simulation was also used in a further simulation observing the sum of PNRs in all possible 4 point combinations to obtain the best 4 point subset: 2kHz/1550°, 20kHz/1550°, 2kHz/750°, 5kHz/750°, hereby referred to as *Protocol 3*. The PNRs were also compared to two protocols used in previous CRI studies involving ex-vivo human patellar cartilage, as referred to as *Protocols 4 and 5* [55], using the qMT values measured in the previous study, fixing T2b to 8μs as did the previous study, and maintaining the SNR for comparison.

In-vivo experiments

The quality of the protocols was tested in in-vivo patella. The knee joint of one volunteer was imaged using *Protocols 1, 2, and 3* with each scan acquired twice to obtain in-vivo measures of patellar cartilage PNR. To validate the consistency of *Protocol 3* (4 point protocol) compared to *Protocol 2* (8 point protocol), the knee joint of one subject was imaged in the axial plane using *Protocols 2* and *3*. For both protocols, qMT parameters were solved in the backward model and then correlated on a point-by-point basis within an ROI covering the entire patellar cartilage. Lastly, the knee joint of one volunteer was imaged using Protocol 3 in the sagittal plane covering the central portion of the tibiofemoral joint in a 30 minute scan time. Just like the previous axial qMT protocol, each MT acquisition utilized a t_m=18ms, TR=42ms, TE=3.5ms, 14 cm FOV, 256 x 256 matrix, and 4 mm slice thickness. Because the qMT model requires knowledge of B_1 and T_1, additional acquisitions were also acquired for an AFI and VFA fitting [62,63]. The signals were then solved in the backward direction to acquire f, k, and T_{2b} cartilage maps of human tibiofemoral joint.

2.4 Results

The PNRs for the digital simulations for *Protocols 1-5* are shown on Table 2-1, and PNRs from imaging human patellar cartilage in-vivo using *Protocols 1-3* are shown in Table 2-2. Point by point correlations in qMT values for human patellar cartilage between *Protocols 2* and *3* showed the following Pearson R correlation coefficients: R_f = 0.988, R_k = 0.852, R_{T2b} = 0.905, R_{PD} = 0.999, R_{R1} = 0.999. qMT images for one slice covering the tibiofemoral condyle are shown in Figure 2-1. A depth-dependent variation in f can be observed in the patellar cartilage, as well as in the tibiofemoral condyle.

Table 2-1. PNR/TERs of digital phantom simulations.

Protocol	PNR_f	PNR_k	PNR_{T2b}	sum(PNR)
1. 8 pts in [6]	15.2	2.44	17.8	35.4
2. Proposed 8 pts	21.2	2.58	24.7	48.6
3. Proposed 4 pts	15.1	2.05	17.3	34.4
4. 27 pts in [2]	12.2	3.72	Fixed	(Fixed T2b)
5. 4 pts in [2]	6.60	.282	Fixed	(Fixed T2b)

Table 2-2. In-vivo PNRs.

Protocol	PNR_f	PNR_k	PNR_{T2b}	PNR
1. 8 pts in [6]	10.9	3.62	13.6	28.2
2. Proposed 8 pt	24.3	3.76	17.8	45.9
3. Proposed 4 pt	15.8	3.59	12.1	31.5

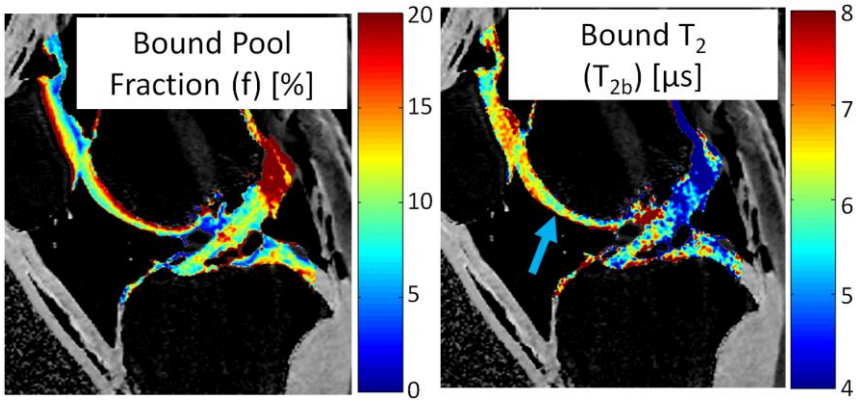

Figure 2-2. Sagittal f map of knee joint shows depth dependent variations of f values in patellar and trochlear cartilage. Corresponding sagittal T_{2b} map shows absence of magic angle effect on T_{2b} values of trochlear cartilage (arrow).

2.5 Conclusions

The digital simulations provide a way to improve qMT parameter quality and have been validated on human patellar cartilage in-vivo. The simulated PNR between protocols seem to align according to the measured PNR calculations, and the proposed 4 point protocol provides comparable performance to the 8 point protocol from the previous study[68]. The protocols from previous ex-vivo studies[55] show lower PNRs (except for PNR_k in *Protocol 4*) possibly because the previous study utilized lower resolutions and likely longer acquisition times in order to maximize SNR. Our study shows that an abbreviated optimized 4-point protocol can provide similar qMT values within patellar cartilage as an optimized 8-point protocol. The reduced scan time makes it more feasible to image the entire knee joint in the sagittal plane, thereby allowing researchers to measure qMT values within both the patellofemoral and tibiofemoral compartment of the knee joint in-vivo.

Chapter 3: Cross Relaxation Parameter Study of In-Vivo Human Patellar Cartilage in Two Subject Populations

Sensitive methods to detect early cartilage degeneration would also be useful in clinical practice to identify the cause of joint pain in symptomatic patients[15] and to allow early initiation of interventions such as weight loss, aerobic activity, and range of motion and strengthening exercises which may alleviate symptoms and potentially slow the rate of joint degeneration[16]. Only one previous study has investigated CRI of articular cartilage which measured f and k in ex-vivo human cadaveric cartilage specimens using a two-pool model that fixed T_2^{B} [55].

In this study, I determine the feasibility and repeatability of using mCRI to detect cartilage degeneration in-vivo within the human knee joint by comparing qMT parameters of patellar cartilage measured using CRI in asymptomatic volunteers and patients with osteoarthritis. In particular, the ability to statistically distinguish mCRI parameters between healthy volunteers and patients with early osteoarthritis is investigated. I also perform an SNR analysis to determine the expected estimation error due to noise.

3.1 Introduction

Modified Cross-relaxation imaging (mCRI) is a qMT method which can acquire three-dimensional parametric maps of articular cartilage measuring the fraction of macromolecular bound protons (f), the exchange rate constant between macromolecular bound protons and free water protons (k), and the T_2 relaxation time of macromolecular bound protons (T_2^{B}) with high

resolution and relatively short scan time based upon a limited number of MT-contrast images[54,56]. Only one previous study has investigated CRI of articular cartilage which measured f and k in ex-vivo human cadaveric cartilage specimens using a two-pool model that fixed T_2^B [55]. I have developed an mCRI protocol for evaluating human patellar cartilage in-vivo at 3.0T which can provide robust measurements of f, k, and T_2^B in a 19 minute scan time. I performed this study to determine the feasibility of using CRI to detect cartilage degeneration within the human knee joint by comparing qMT parameters of patellar cartilage measured using CRI in asymptomatic volunteers and patients with osteoarthritis.

3.2 Methods

Cross-Relaxation Imaging Protocol

CRI relies on a previously developed mathematical model describing magnetization exchange between macromolecular bound protons and free water proton pools which takes into account the effects of excitation and off-resonance MT saturation pulses on spoiled gradient recall-echo (SPGR) sequences[34,54]. In this approach, the saturation of the free water proton pool is minimized by utilization of off-resonance MT saturation pulses sufficiently far from resonance. Our particular implementation employs a modified CRI model for accurate modeling of the relaxation effects while minimizing the number of scans needed for the model fit[56]. The model requires several SPGR datasets with and without magnetization preparatory pulses acquired over a range of offset frequencies, saturation powers (i.e. MT flip angles), and excitation flip angles to measure the qMT parameters f, k, and T_2^B.

In order to optimize the experiment design, Monte-Carlo simulations were first performed to determine the combinations of MT offset frequencies, MT flip angles, and excitation flip angles which maximized parameter-to-noise ratio (PNR) for f, k, and T_2^B of cartilage while maintaining a clinically feasible scan time. The resulting CRI protocol consisted of six MT-prepared SPGR scans and four non-MT-prepared SPGR scans. The MT-prepared SPGR scans were performed with different combinations of MT offset frequencies and flip angles (2.5 kHz/1550^o, 5 kHz/1550^o, 10 kHz/1550^o, 20 kHz/1550^o, 2.5 kHz/890^o, and 5 kHz/890^o) with an 18-ms Fermi MT pulse, 42 ms repetition time, 3.2 ms echo time, and 13^o excitation flip angle. The non-MT-prepared SPGR scans were performed over a range of excitation flip angles (4^o, 10^o, 20^o, and 30^o) with a 24 ms repetition time and 3.2 ms echo time. Actual flip angle imaging (AFI) was also performed for flip angle mapping using an SPGR scan consisting of two identical radiofrequency pulses followed by repetition times of 30 ms and 150 ms acquired with a 2.2 ms echo time and 55^o excitation flip angle[62]. All SPGR scans were performed using a 31 kHz bandwidth, 14 cm field of view, 256 x 256 matrix for the MT-prepared and non-MT-prepared scans and 128 x 128 matrix for the AFI scans, 4 mm slice thickness, 10 slices, and one signal average. Total scan time for the CRI protocol was 19 minutes. In order to measure MTR, one additional MT-prepared SPGR scan was performed using the same imaging parameters except for a 250 kHz offset frequency and 1550^o flip angle to create negligible MT effect.

Study Group

The study was performed in compliance with HIPAA regulations and with approval from our Institutional Review Board. All subjects signed informed consent prior to their participation in the study. The study group consisted of 20 asymptomatic volunteers (15 males and five females between 23 and 45 years of age with an average age of 32.3 years) and 11 patients with osteoarthritis of the knee joint (seven males and four females between 45 and 62 years of age with an average age of 52.6 years). All patients with osteoarthritis of the knee joint were diagnosed by a fellowship trained sports medicine specialist using standardized criteria which included complaints of chronic knee pain and stiffness for a minimum of six months and the presence of definitive grade 2 osteophytes on standing anterior-posterior radiographs of the knee[70,71]. All patients had mild osteoarthritis within the patellofemoral compartment with 6 patients showing small grade 1 osteophytes and 5 patients showing definitive grade 2 osteophytes on the patella and femoral trochlea and no patients showing joint space narrowing on axial radiographs of the knee[72].

MR Examination

An MR examination of the knee joint was performed on all subjects in the study group using a 3.0T scanner (Discovery MR750, GE Healthcare, Waukesha, WI) and an 8-channel phased-array extremity coil (In Vivo, Orlando, FL). Foam padding was used to firmly secure the knee within the coil to minimize subject motion during the MR examination. All MR examinations consisted of the following sequences performed in the axial plane through the patellofemoral compartment of the knee joint: 1) the CRI protocol described in the previous section, 2) a frequency-selective

fat-suppressed T2-weighted fast spin-echo sequence acquired using a 4050 ms repetition time, 85 ms echo time, 90^{o} excitation flip angle, 31 kHz bandwidth, 14 cm field of view, 256 x 256 matrix, 4 mm slice thickness, and four signal averages, and 3) an SPGR sequence with iterative decomposition of water and fat with echo asymmetry and least-squares estimation (IDEAL) fat-water separation[73] acquired using a 12.4 ms repetition time, 3.4 ms, 4.2 ms, and 5.0 ms echo times, 14^{o} excitation flip angle, 31 kHz bandwidth, 14 cm field of view, 256 x 256 matrix, 4 mm slice thickness, and one signal average. A frequency-selective fat-suppressed three-dimensional intermediate-weighted fast spin-echo sequence was also performed in the sagittal plane through the knee joint using a 2217 ms repetition time, 23.6 ms echo time, 90^{o} excitation flip angle, 31 kHz bandwidth , 15 cm field of view, 256 x 256 matrix, 1 mm slice thickness, and one signal average. Coronal and axial reformat images were created from the volumetric fast spin-echo source data.

Cartilage qMT Parameter Map Reconstruction

Quantitative MR parameter maps of patellar cartilage were reconstructed using in-house software developed in MATLAB (MATLAB 2011b, MathWorks Inc, Natick, MA). Image registration software (FLIRT, Functional Magnetic Resonance Imaging of the Brain Analysis Group, Oxford University, United Kingdom) was used to correct for any subject motion which may have occurred between the multiple scans. The MT-prepared and non-MT-prepared SPGR datasets were simultaneously fitted on a pixel-by-pixel basis using a non-linear least squares two-pool model to create cartilage f, k and T_2^B maps[56]. Both excitation flip angle and MT saturation power were corrected for each pixel using the flip angle maps acquired from the AFI

scans. In addition, cartilage MTR maps were created using a pixel-by-pixel measurement of the difference in the signal of the SPGR scan with negligible MT effect (250kHz/1550^{o}) and the SPGR scan with strongest MT effect (2.5kHz/1550^{o}) divided by the signal of the SPGR scan with negligible MT effect[28,74].

Comparison of Morphologic and Quantitative MR Parameters Between Groups of Subjects

Morphologic joint analysis was performed by a fellowship-trained musculoskeletal radiologist with 12 years of clinical experience who was blinded to whether a subject was an asymptomatic volunteer or patient with osteoarthritis. The radiologist used the axial fat-suppressed T2-weighted fast spin-echo, axial IDEAL-SPGR, and multi-planar fat-suppressed three-dimensional intermediate-weighted fast spin-echo images to grade the severity of degeneration within the knee joint using the Boston-Leeds Osteoarthritis Knee (BLOK) scoring system[75]. A patellar BLOK score and total knee BLOK score was measured for each subject using the semi-quantitative scoring system.

Quantitative cartilage analysis was performed by a research assistant with four years of cartilage segmentation experience under the supervision of the fellowship-trained musculoskeletal radiologist using software developed in MATLAB (MATLAB 2011b, MathWorks Inc, Natick, MA). Regions of interest were placed around the patellar cartilage on each slice of the IDEAL-SPGR images of each subject to create a three-dimensional contour of patellar cartilage. The three-dimensional contour was then superimposed over the cartilage MTR, f, k, and T_2^B maps to measure the average quantitative MR parameters of patellar cartilage.

Non-parametric two-tailed Mann-Whitney-Wilcoxon rank-sum tests were used to compare MTR, f, k, and T_2^B of patellar cartilage between asymptomatic volunteers and patients with osteoarthritis. The Bonferonni method was used to account for comparison of multiple quantitative MR parameters between groups of subjects. Statistical significance was defined as a p-value less than 0.01 using a standard p-value cut-off of 0.05 and a comparison of four quantitative MR parameters between asymptomatic volunteers and patients with osteoarthritis.

Assessment of Repeatability of Cartilage Quantitative MR Measurements

The CRI protocol was performed twice on both knee joints of five asymptomatic volunteers (five males between 28 and 32 years of age with an average age of 29.2 years) with the subjects taken out of the scanner and allowed to rest in a sitting position for 10 minutes between the scans for a total of four scans per subject. Average MTR, f, k, and T_2^B of patellar cartilage were measured using the previously described methods. Repeatability of cartilage quantitative MR measurements was assessed using coefficient of variance which was defined as the standard deviation divided by the average of the cartilage parameters obtained using the two scans performed on the same knee of the same subject. Confidence intervals for coefficient of variance were calculated using the approximate pivotal method. Bland-Altman analysis was also performed to assess the estimated bias and 95% limits of agreement between the cartilage measurements obtained using the two CRI scans.

Assessment of Signal-to-Noise Ratio (SNR) of the CRI Protocol

Monte Carlo simulations were used to compare the signal-to-noise ratio (SNR) to the variations due to error in MTR, f, k, and T_2^B [76]. One hundred digital phantoms, each containing 2000 pixels, were created using the average MTR, f, k, and T_2^B of all subjects in the study. Different levels of normally distributed noise were added to the digital signals to simulate SNR levels from 0 to 160 in increments of 20. For each SNR level, the digital phantom data was used to obtain estimates of MTR, f, k, and T_2^B [56]. The average MTR, f, k, and T_2^B were calculated over each digital phantom at each SNR level. Standard deviations of the averages were taken at each SNR level. The standard deviations were then normalized as a percentage of the average MTR, f, k, and T_2^B values. The results were compared to the observed differences in MTR, f, k, and T_2^B between asymptomatic volunteers and patients with osteoarthritis at the reference SNR for the CRI protocol. The reference SNR for the CRI protocol was determined using the addition/subtraction method in which two identical SPGR scans with negligible MT effect were performed on an asymptomatic volunteer one immediately following the other. Signal was defined as the signal of patellar cartilage on the addition images divided by 2, while noise was defined as the standard deviation of patellar cartilage on the subtraction images divided by the square root of 2 [77].

3.3 Results

All asymptomatic volunteers had a patellar BLOK score and total knee BLOK score of 0 indicating no degeneration within the knee joint. Patients with osteoarthritis had patellar BLOK scores ranging between 6 and 13 with an average value of 8.0 and total knee BLOK scores

ranging between 27 and 58 with an average value of 36.1. All patients with osteoarthritis had osteophytes and focal areas of partial-thickness cartilage loss on the patella with two patients also having subchondral bone marrow edema.

Figure 3-1 shows box plots illustrating the distribution of MTR, f, k, and T_2^B values of patellar cartilage for asymptomatic volunteers and patients with osteoarthritis. Average MTR, f, k, and T_2^B of patellar cartilage was 0.62 (95% confidence intervals 0.62 to 0.63), 12.46% (95% confidence intervals 12.32% to 12.93%), 7.22 s^{-1} (95% confidence intervals 6.57 s^{-1} to 7.56 s^{-1}) and 6.49 μs (95% confidence intervals 6.45 μs to 6.60 μs) respectively for asymptomatic volunteers and 0.62 (95% confidence intervals 0.62 to 0.64), 12.80% (95% confidence intervals 12.16% to 13.09%), 6.13 s^{-1} (95% confidence intervals 5.86 s^{-1} to 6.85 s^{-1}), and 6.80 μs (95% confidence intervals 6.63 μs to 6.87 μs) respectively for patients with osteoarthritis. There was significantly lower k ($p<0.01$) and significantly higher T_2^B ($p<0.0001$) of patellar cartilage in patients with osteoarthritis than asymptomatic volunteers. There was no significant difference in MTR ($p=0.52$) and f ($p=0.38$) of patellar cartilage between groups of subjects. **Figures 3-2**, **3-3**, and **3-4** illustrate examples of differences in the qMT parameters f, k, and T_2^B of patellar cartilage between asymptomatic volunteers and patients with osteoarthritis.

Figure 3-1

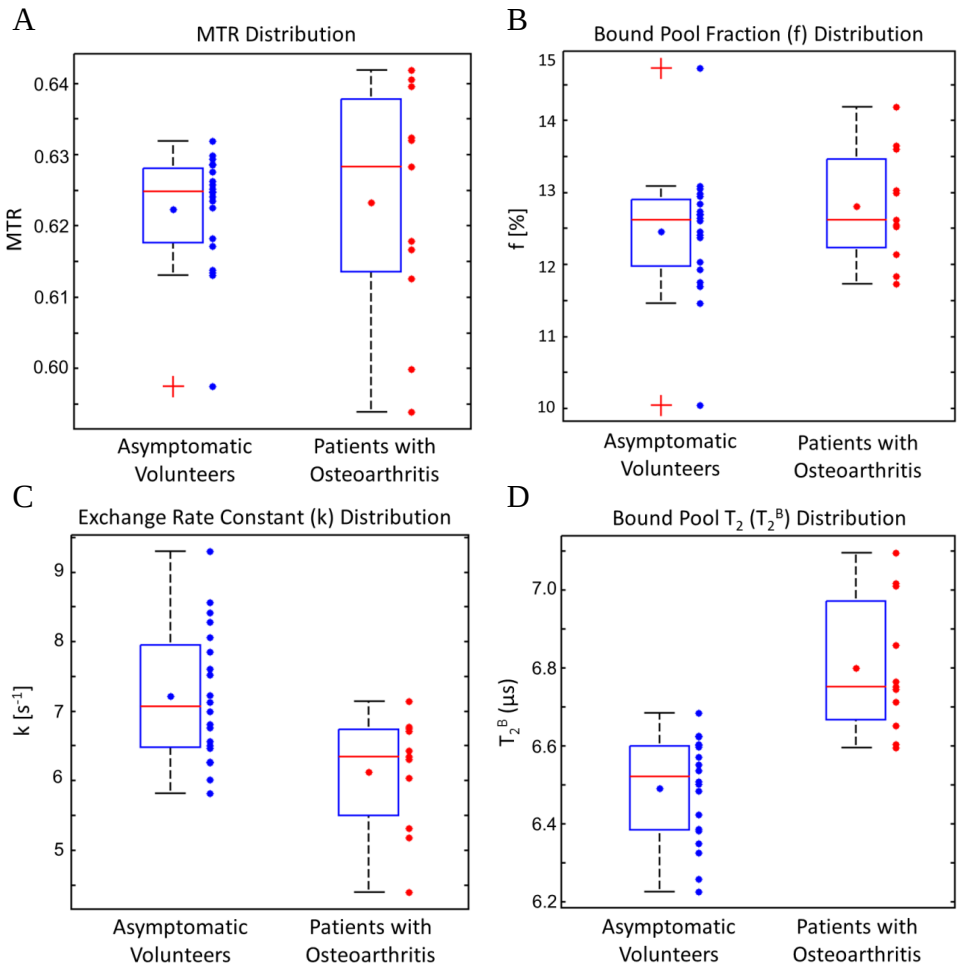

Figure 3-1: Box plots illustrating the distribution of (A) MTR, (B) f, (C) k, and (D) T_2^B values of patellar cartilage in asymptomatic volunteers and patients with osteoarthritis. The boxes indicate interquartile ranges, the blue dots within the boxes indicate average values, the red lines within the boxes indicate median values, the whiskers extend to the most extreme data points not considered outliers (1.5 of the interquartile range between the first and third quartiles), and the crosses indicate outliers.

Figure 3-2

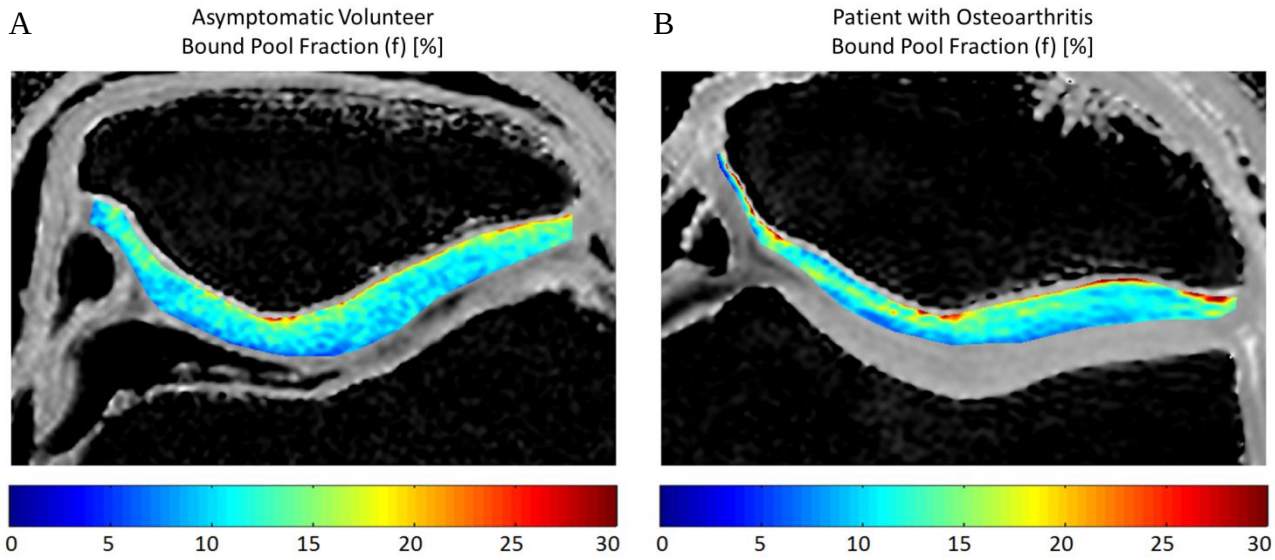

Figure 3-2: Comparison of f of patellar cartilage in (A) a 25 year old male asymmetric volunteer and (B) a 52 year old male patient with osteoarthritis. Note that there are no visible differences in f between the asymptomatic volunteer and the patient with osteoarthritis.

Figure 3-3

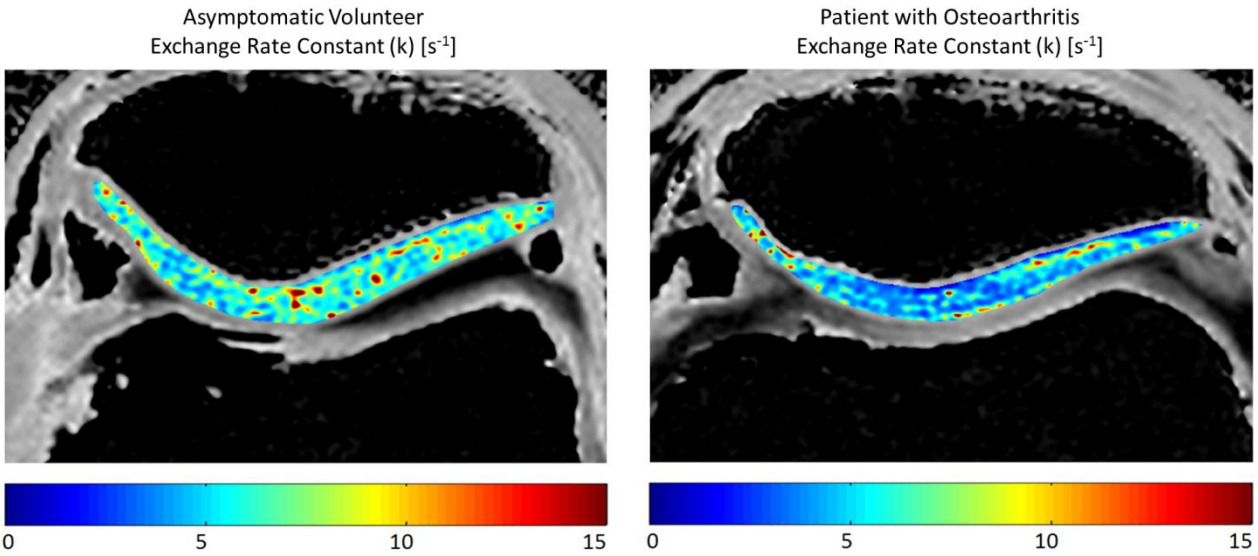

Figure 3-3: Comparison of k of patellar cartilage in (A) a 27 year old male asymmetric volunteer and (B) a 45 year old male patient with osteoarthritis. Note that the patient with osteoarthritis has lower k of patellar cartilage than the asymptomatic volunteer.

Figure 3-4

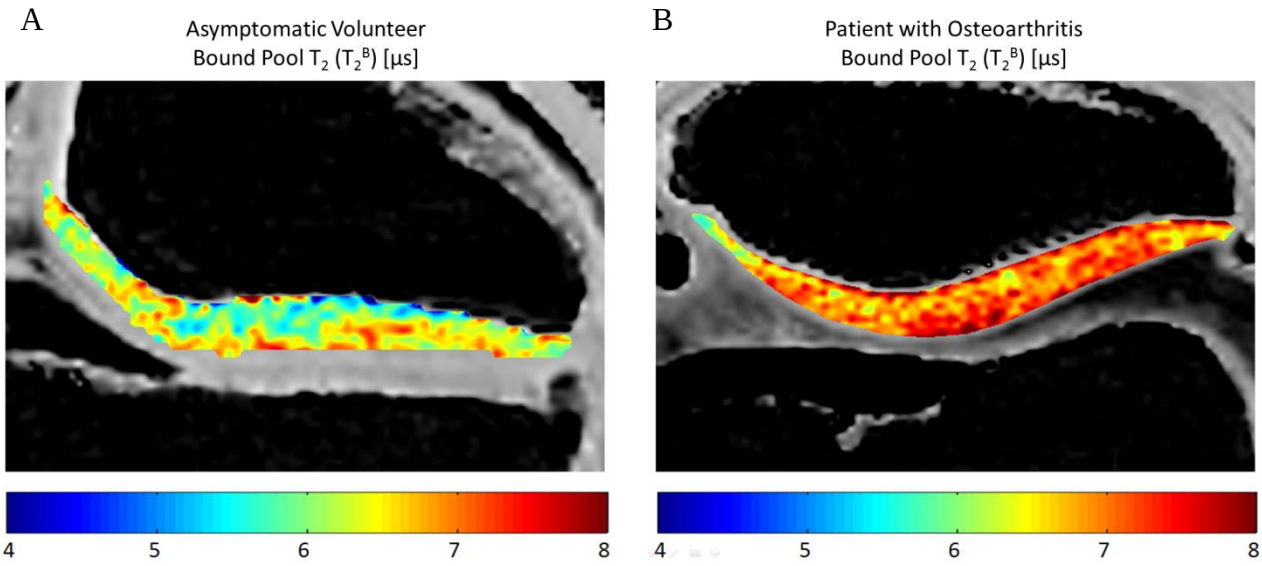

Figure 3-4: Comparison of T_2^B of patellar cartilage in (A) a 27 year old male asymmetric volunteer and (B) a 45 year old male patient with osteoarthritis. Note that the patient with osteoarthritis has higher T_2^B of patellar cartilage than the asymptomatic volunteer.

Figure 3-5

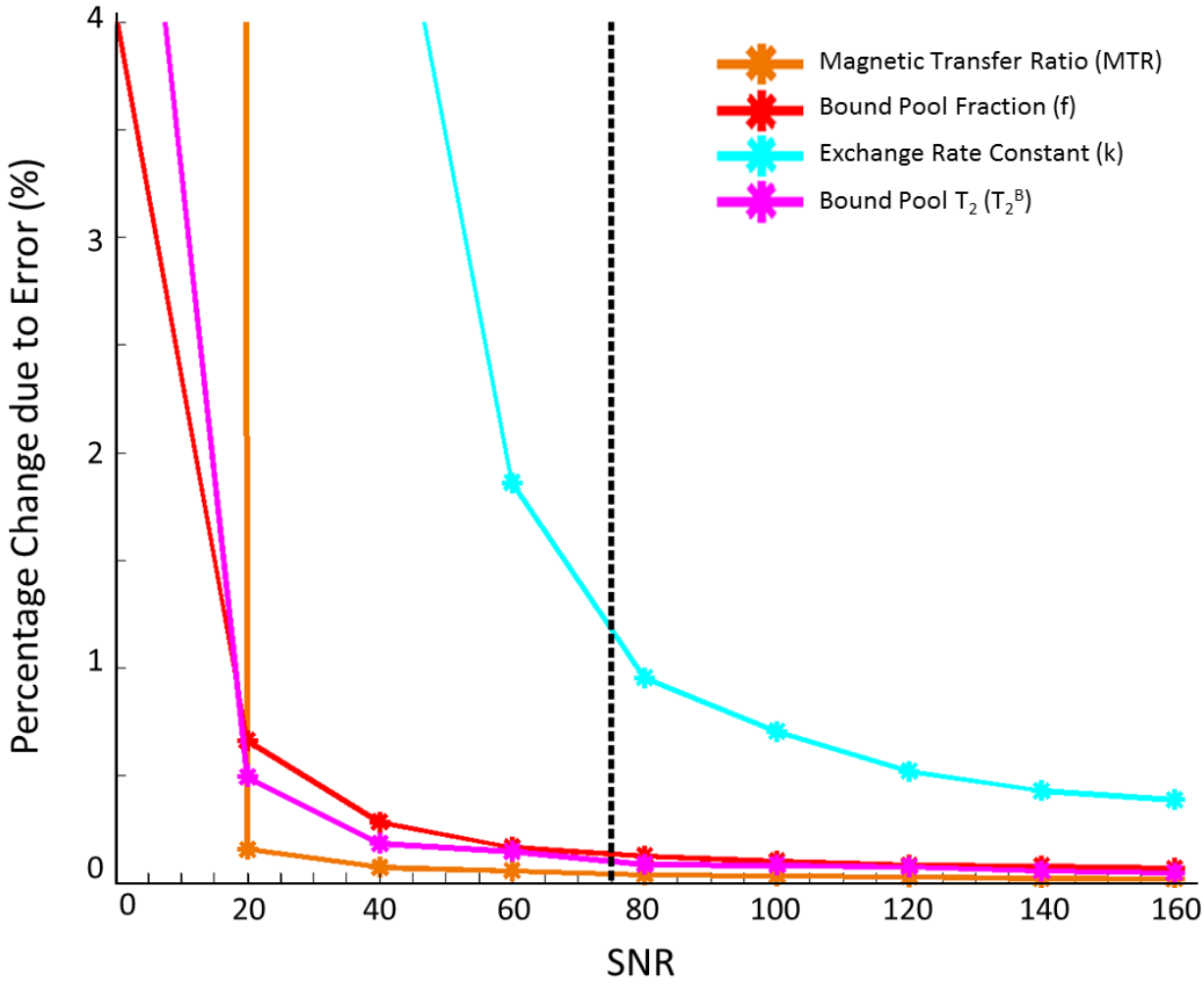

Figure 3-5: Relationship between normalized standard deviation due to error and SNR for MTR, f, k, and T_2^B of patellar cartilage. The reference SNR of 75 for the CRI protocol (dotted black vertical line) provides low percent change due to error in all quantitative MR parameters.

Coefficients of variance for repeat quantitative MR measurements obtained using the two CRI scans performed on the same knee of the same subject were 0.45% for MTR (95% confidence intervals 0.44% to 0.48%), 2.21% for f (95% confidence intervals 2.15% to 2.35%), 4.56% for k (95% confidence intervals 4.44% to 4.87%), and 0.72% for T_2^B (95% confidence intervals 0.70% to 0.77%). The estimated bias for repeat measurements on Bland-Altman analysis were 0.01 for MTR, -0.24 for f, -0.05 for k, and 0.02 for T_2^B, while the 95% limits of agreement were -0.01 to 0.02 for MTR, -1.08 to 0.50 for f, -1.58 to 1.47 for k, and -0.14 to 0.17 for T_2^B.

The relationships between signal-to-noise ratio (SNR) and variations due to error in MTR, f, k, and T_2^B are illustrated in **Figure 3-5**. The normalized standard deviation for a given parameter may be interpreted as the percent change expected due to noise and data fit instability at a certain SNR level. At the reference SNR of 75 for the CRI protocol, the percent change expected due to noise and data fit instability was approximately 0.1% in MTR, 0.1% in f, 1% in k, and 0.1% in T_2^B. In comparison, the percent change of the differences in qMT values of patellar cartilage between asymptomatic volunteers and patients with osteoarthritis was 0.1% for MTR, 2.8% in f, -15.9% in k, and 4.7% in T_2^B.

3.4 Discussion

Our study has demonstrated the feasibility of using CRI to measure the qMT parameters f, k, and T_2^B of the articular cartilage of the knee joint in human subjects which has never been previously performed to the best of our knowledge. Our study found significant differences in f and T_2^B of patellar cartilage between asymptomatic volunteers and patients with osteoarthritis which

indicates that qMT parameters measured using CRI can detect cartilage degeneration within the human knee joint. MTR could not distinguish between groups of subjects which is similar to the findings of a previous study which found no significant difference in MTR of patellar cartilage between asymptomatic volunteers and patients with osteoarthritis[78(p1)]. These results suggest that a more detailed analysis of the magnetization exchange between macromolecular bound protons and free water protons provided by CRI is needed to detect changes in the macromolecular matrix of degenerative cartilage.

Our study found significantly lower k and significantly higher T_2^B of patellar cartilage in patients with osteoarthritis when compared to asymptomatic volunteers. Few previous studies have investigated k and T_2^B of cartilage, and thus the exact mechanisms of the observed changes in the qMT parameters remain unknown. However, previous ex-vivo studies have shown that k decreases[79,80] and T_2^B increases[79] with proteoglycan loss due to trypsin degradation of bovine cartilage specimens. Furthermore, thermal denaturation of collagen solution has been shown to cause an increase in T_2^B although the change was accompanied by a decrease in f[79]. Thus, the decrease in k and increase in T_2^B with cartilage degeneration in our study may be due to the combined effects of proteoglycan loss and collagen denaturation which both occur during the early stages of osteoarthritis [11–13]. Fragmentation of collagen, which decreases proton binding sites on the macromolecule, and loss of bulk water from cartilage due to decreased proteoglycan content may reduce the exchange rate between macromolecular-bound and free water protons. Fragmentation of collagen may also increase the mobility of the macromolecule within cartilage and thereby increase T_2^B. Decreased organization of the cartilage matrix due to collagen

denaturation and proteoglycan loss may increase spin diffusion of macromolecular-bound protons, the primary mechanism defining T_2 relaxation time in the semisolid fraction, and thereby also increase T_2^B [65].

Our study found no significant difference in f of patellar cartilage in patients with osteoarthritis when compared to asymptomatic volunteers. The factors responsible for the measured f values of cartilage are incompletely understood. A previous study using CRI to investigate ex-vivo human cadaveric cartilage specimens found a moderate correlation between f and the proteoglycan content of cartilage[55]. However, the two-pool model used in the study fixed T_2^B which has been shown in our study to change with cartilage degeneration. Another study using proteoglycan and collagen phantoms and a similar CRI protocol as our study has documented large increases in f with increasing collagen concentration but only negligible increases in f with increasing proteoglycan concentration. The same study found no change in f with proteoglycan loss due to trypsin degradation of ex-vivo bovine cartilage specimens suggesting that proteoglycan content has a minimal effect on f [79]. Proteoglycan has an abundance of macromolecular bound protons, but its concentration within cartilage is lower[11] and its protons are more mobile[81] when compared to collagen which may limit its contribution to f. The absence of changes in f with cartilage degeneration in our study may be due to the fact that f is primarily a measure of the collagen content of cartilage which decreases by only 5% during the late stages of osteoarthritis[44]. However, additional studies are needed to investigate the influence of collagen and proteoglycan on the measured f values of both normal and degenerative cartilage.

The CRI protocol used in our study had adequate SNR to detect differences in qMT parameters between groups of subjects and high repeatability with coefficients of variance which compared favorably with other quantitative cartilage imaging techniques[82–84]. However, k was more sensitive to measurement errors when compared to f and T_2^B with lower repeatability and higher percent change expected due to noise and data fit instability. These results are consistent with the findings of a previous study investigating qMT parameters within neural tissue which showed that small fluctuations in MT signals due to measurement error had a more significant effect on k than f and T_2^B [66]. One method to improve measurements of k of articular cartilage would be to acquire SPGR scans at higher MT flip angles than those used in our study. However, using higher MT flip angles would increase specific absorption rate (SAR) so SAR would need to be reduced by using lower field strength scanners at the expense of decreased SNR or longer repetition times at the expense of increased scan time.

Our study has several limitations. One limitation was the relatively small number of subjects which prevented detailed analysis of inter-group variability in qMT parameters and identification of thresholds for k and T_2^B which could be considered diagnostic for cartilage degeneration. Another limitation was that not all patients with osteoarthritis in our study had definitive grade 2 osteophytes within the patellofemoral compartment which is considered to be the radiographic hallmark of the disease[71]. However, all patients did have osteoarthritis of the whole knee joint diagnosed using standardized clinical and radiographic criteria[70,71]. Furthermore, a group of patients with mild osteoarthritis within the patellofemoral compartment was desired to determine whether CRI could detect early cartilage degeneration of the patella. Another limitation of our

study was that it could not identify the mechanisms responsible for changes in k and T_2^B between asymptomatic volunteers and patients with osteoarthritis. Additional studies with histopathologic correlation are needed to investigate the factors responsible for changes in qMT parameters at various stages of cartilage degeneration. A final limitation was that the CRI protocol used in our study had a relatively long scan time which limited qMT assessment to 10 slices through patellar cartilage. We are currently investigating various methods to reduce the scan time of the CRI protocol including use of a smaller number of optimized magnetization preparatory pulses, more rapid methods for flip angle mapping, and compressed sensing with parallel imaging to provide complete anatomic coverage of the knee joint in the sagittal plane.

In conclusion, our study has shown that patients with osteoarthritis have significantly lower k and significantly higher T_2^B of patellar cartilage than asymptomatic volunteers which indicates that qMT parameters measured using CRI can detect cartilage degeneration within the human knee joint. CRI may provide a new quantitative MR technique to identify patients with early cartilage degeneration and to monitor disease-related and treatment-related changes in the macromolecular matrix of articular cartilage in osteoarthritis research studies. However, further studies are needed to better understand the fundamental mechanisms responsible for changes in qMT parameters in patients with osteoarthritis and to identify thresholds of k and T_2^B which could be considered diagnostic for cartilage degeneration.

Chapter 4: Methods for Measuring the Stability and Biological Significance of Cross Correlation Parameters using Ex-Vivo Pre-clinical Models

The biological context for changes in qMT parameters is of utmost interest, and this work is also devoted to mCRI protocol development for ex-vivo cartilage applications. For instance, degradation studies may provide further understanding about how parametric maps may change with changes in macromolecular content or cartilage ultrastructure. Compared to in-vivo human cartilage studies, ex-vivo cartilage animal model studies merit different mCRI protocols, due to several key differences in cartilage morphology and study design.

This chapter serves to describe the methods used to develop and validate an mCRI protocol for ex-vivo cartilage tissue at 3.0T.

4.1 Introduction

Osteoarthritis research is stemmed in cartilage biology: cartilage degeneration involves changes in macromolecular content and microstructure. These changes involve collagen mesh network characteristics, collagen content, and proteoglycan content of the cartilage. The significant prevalence of osteoarthritis in the human population motivates the need to understand cartilage degradation using non-invasive, non-destructive techniques, and magnetic resonance imaging may be an attractive imaging modality for its soft tissue contrast. However, the signal from MRI

is conventionally focused on changes in water protons: e.g., contrast due to T_1-weighting, T_2-weighting, and proton density weighting.

Studies have shown that morphological changes in cartilage succeed irreversible biochemical and structural changes in the tissue [6,9]. One study showed that while there was no visible morphological change in the knee cartilage, physical probing areas of the cartilage with a metallic probe revealed softening of the cartilage. [10] This suggests that qualitative, morphologic MR imaging of cartilage would not be sufficient to detect changes due to early OA. While qualitative MRI is suitable for detecting acute changes, it is insufficient in measuring slow, chronic changes as characterized by OA. OA is a measurement problem, not a detection problem.

In contrast, quantitative MRI seeks to measure physical properties such that the value of each voxel corresponds to a meaningful metric obtained from a theoretical model. Quantitative Magnetization Transfer (qMT) is particularly attractive, since the MR signal is obtained via macromolecular contrast through the magnetization transfer (MT) effect. qMT can further be performed on a conventional 1.5T or 3T MR scanner, and does not require specialized hardware, unlike several other quantitative MRI techniques.

Modified Cross-relaxation imaging (mCRI) is a quantitative magnetization transfer (qMT) method which can acquire three-dimensional parametric maps of articular cartilage measuring the fraction of macromolecular bound protons (f), the exchange rate constant between

macromolecular bound protons and free water protons (k), and the T_2 relaxation time of macromolecular bound protons (T_2^B) with high resolution and relatively short scan time based upon a limited number of MT-contrast images [54,56].

The extracellular matrix (ECM) of the cartilage makes up the tissue's main constituent macromolecules and is responsible for cartilage structure and function [6,9]. The most prominent macromolecule in the cartilage microstructure is collagen. Type II collagen makes up 15-20% of the wet weight [6,9]. Collagen provides the structural framework for the matrix [6]. The collagen fibers form an intricate structure that can be divided into different layers according to the depth of the cartilage from the articular surface [9].

Another large macromolecular contributor to the wet weight of the cartilage is aggrecan. Aggrecans are large aggregating molecules of proteoglycans (PGs), and make up 3-10% of the weight in articular cartilage [9]. Aggrecan also contains a complex with a protein core with an extended domain that links many glycosaminoglycan (GAG) side chains [9]. In physiologic conditions, the GAGs are densely packed and exhibit a strong negative charge of around as much as 150mM to 300mM in normal articular cartilage [9]. GAG depletion can be used as an early biomarker to detect OA progression [6,9]. In later stages of OA, there is near complete loss of PG[6].

Compared to in-vivo human cartilage studies, ex-vivo cartilage animal model studies merit different mCRI protocols, due to several key differences in cartilage morphology and study design. First, ex-vivo patellar cartilage from animal models is typically thinner than healthy

human cartilage. The thickness of bovine cartilage can vary based on a wide variety of factors, including age, weight, and breed. The difference in cartilage thickness necessitates a higher resolution to obtain usable voxels for quantitative analysis. Additionally, to maintain an acceptable SNR for quantitative analysis, slice resolution is typically low, but low slice resolutions also increase the potential error due to partial voluming. At lower cartilage thickness, this partial voluming effect can become increasingly severe. Thus, the slice resolution for ex-vivo cartilage must be higher than the slice resolution for in-vivo cartilage, while managing the tradeoff in SNR.

Significant care must also be taken to correctly position the ex-vivo cartilage, due largely to this typically thinner tissue. For instance, relatively high slice thicknesses can cause significant partial voluming from any curvature of the cartilage in the z-direction of the magnet. This curvature can manifest itself in the natural configuration of the tissue (as the patella is naturally curved) and also in any tilting in the z-direction. Different studies may also contribute to this potential curvature. For instance, magic angle studies inherently require that the cartilage be oriented at different angles in the X-Y plane, but these changes require manual repositioning, so it is impossible to perfectly ensure that the curvature in the z-direction is the same at every repositioning (though we can come close).

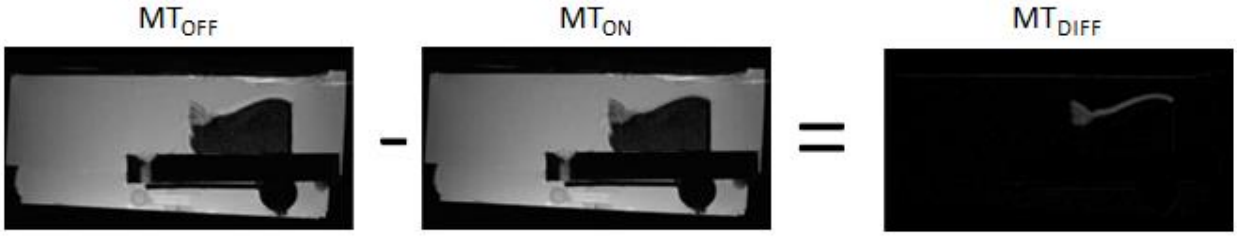

Figure 4-1. PBS fluid from sample prep and fat from patellar bone do not exhibit significant MT effect. The difference between an MT-weighted image with an MT without MT weighting can create a sparse environment and remove unwanted signal from voxels not exhibiting an MT effect.

To maintain hydration and minimize B_0 error, ex-vivo cartilage needs to be immersed in phosphate buffered saline (PBS) solution. Conversely, the surrounding environment for in-vivo patellar cartilage is typically very heterogenous—depending on the location of the voxel, patellar cartilage may be adjoined by interstitial fluid, skin, or other cartilage surfaces. The relatively increased predictability of the ex-vivo tissue environment allows for the potential to exploit the fact that PBS and bone do not exhibit an MT effect (**Figure 4-1**). On the other hand, the difference in tissue environments also creates significant differences in B_1 distribution.

Differences in study design also demand increased imaging requirements. For instance, degradation studies for ex-vivo animal models expectedly erode the surface of the cartilage and results in even thinner morphology after treatment. This thinner morphology further demands higher in-plane resolution and also increases the potential effect of partial voluming. Additionally, the goals of ex-vivo and in-vivo cartilage studies are similar, but fundamentally

different. My in-vivo cartilage study aimed to distinguish population differences between asymptomatic volunteers and patients with osteoarthritis, while minimizing the required scan time. This in-vivo study inherently cannot track the progression of disease, since it can only predict differences in cartilage composition and microstructure. However, ex-vivo studies have the greater potential to directly observe changes in cartilage composition and microstructure by inducing changes to the cartilage and observing mCRI parameters before and after these changes. This greater potential demands a higher level of accuracy, and scan time can be considerably increased to provide higher SNR. Estimation accuracy may be further improved by optimizing the protocol to determine which MT points provide the greatest contribution in accurately calculating mCRI parameters. These optimal MT points may change due to differences in human and animal cartilage tissue composition, microstructure, and environment.

One previous study has investigated CRI of articular cartilage which measured f and k in ex-vivo human cadaveric cartilage specimens using a two-pool model that fixed T_2^{B} [55]. However, I found that T_2^{B} changes significantly between asymptomatic volunteers and patients with osteoarthritis, so it is critical to understand the changes in f, k and, T_2^{B} in the context of macromolecular changes in structure and content. Toward this goal and the above mentioned imaging considerations, I developed an mCRI protocol for evaluating ex-vivo cartilage at 3.0T for animal models, which can provide robust measurements of f, k, and T_2^{B} with higher resolution, wider coverage, and higher SNR.

4.2 Theory

Modified Cross-Relaxation Imaging

CRI relies on a previously developed mathematical model describing magnetization exchange between macromolecular bound protons and free water proton pools which takes into account the effects of excitation and off-resonance MT saturation pulses on spoiled gradient recall-echo (SPGR) sequences [34,54]. In this approach, the saturation of the free water proton pool is minimized by utilization of off-resonance MT saturation pulses sufficiently far from resonance. Our particular implementation employs a modified CRI model for accurate modeling of the relaxation effects while minimizing the number of scans needed for the model fit [56]. The model requires several SPGR datasets with and without magnetization preparatory pulses acquired over a range of offset frequencies, saturation powers (i.e. MT flip angles), and excitation flip angles to measure the qMT parameters f, k, and T_2^B.

Magnetization Transfer Subtraction

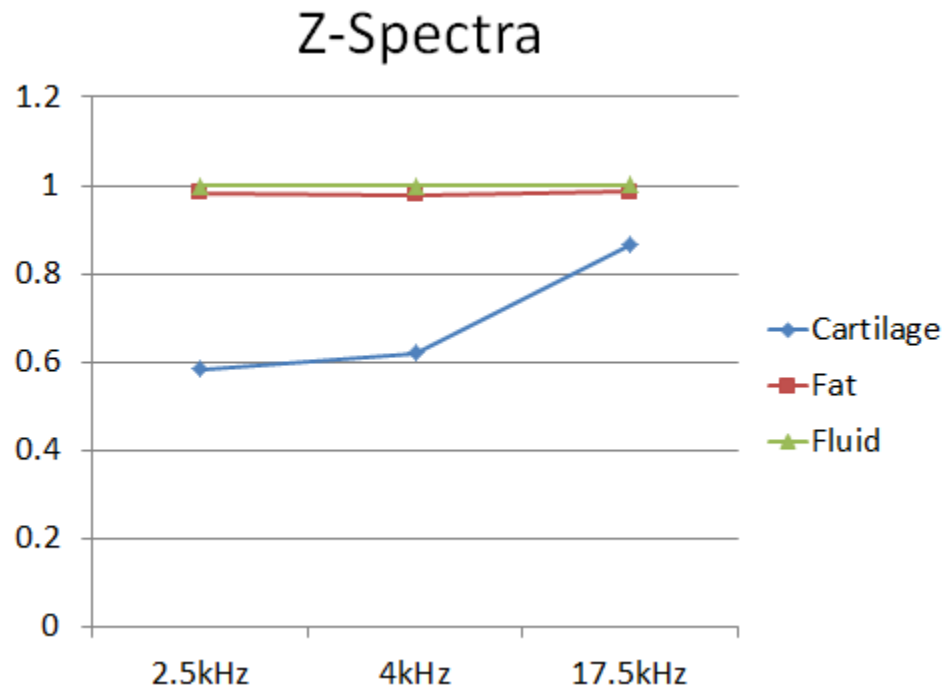

Figure 4-2. Z-Spectra of various regions in the ex-vivo imaging environment. Fluid signal corresponds to regions with PBS. Fat signal corresponds to regions inside patellar bone. Cartilage signal exhibits an MT effect, so its z-spectra shows decreasing amounts of saturation with increasing MT offset frequency. In contrast, the z-spectra of fat and fluid is relatively flat.

Two MT images, one with negligible MT effect ($\mathbf{MT_{OFF}}$) and another with significant MT effect ($\mathbf{MT_{ON}}$), can be subtracted ($\mathbf{MT_{DIFF}} = \mathbf{MT_{OFF}} - \mathbf{MT_{ON}}$) to remove fat and PBS signal and create a sparse image for tissue environments rich in fat (**Figure 4-1**). Therefore, in voxels where partial voluming or chemical shift is present, $\mathbf{MT_{DIFF}}$ contains no signal contribution from fat or PBS (**Figure 4-2**). mCRI utilizes an array of $\mathbf{MT_{ON}}$ signals to obtain bound pool fraction (f),

exchange rate constant (k), and transverse bound pool T_2 (T_2^B), as well as proton density and T_1 [56]. However, mCRI can be modified to utilize an array of $\mathbf{MT_{DIFF}}$ signals instead, by fitting the qMT parameters with $\mathbf{MT_{OFF}}$ - $\mathbf{MT_{ON}}$.

Normally, the z-spectra is calculated by the formal relationship,

$$Z(x,y) = \frac{MT_{ON}(x,y)}{MT_{OFF}(x,y)}$$

However, when the MT weighted signals are corrupted with non-exchanging signal (such as fat or PBS fluid), the formal relationship includes a DC offset in both the numerator and denominator:

$$Z(x,y) = \frac{MT_{ON}(x,y) + S_{DC}(x,y)}{MT_{OFF}(x,y) + S_{DC}(x,y)}$$

It is important to note here that the value of S_{DC} will strongly depend on the species of the signal (fat or fluid). If the species is fat, then S_{DC} can be negative when there is an out-of-phase relationship between fat and H_2O for spoiled gradient echo sequences.

4.2 Methods

Protocol Development

In order to optimize the experiment design, Monte-Carlo simulations were first performed[85] to determine the combinations of MT offset frequencies, MT flip angles, and excitation flip angles which minimized the normalized variance[86] for f, k, and T_2^B of ex-vivo bovine cartilage. The resulting mCRI protocol consisted of 8 MT-prepared SPGR scans and 4 non-MT-prepared SPGR

scans. The MT-prepared SPGR scans were performed with different combinations of MT offset frequencies and flip angles (2.5kHz/500°, 2.5kHz/600°, 4kHz/600°, 4kHz/700°, 2.5kHz/1400°, 2.5kHz/1550°, 4kHz/1550°, 17.5kHz/1550°) with an 18-ms Fermi MT pulse, 45 ms repetition time, 5.1 ms echo time, 13^{o} excitation flip angle, and 3 signal averages. The non-MT-prepared SPGR scans were performed over a range of excitation flip angles (6^{o}, 15^{o}, 25^{o}, and 33^{o}) with a 24 ms repetition time, 5.1 ms echo time, and 1 signal average. Actual flip angle imaging (AFI) was also performed for flip angle mapping using an SPGR scan consisting of two identical radiofrequency pulses followed by repetition times of 30 ms and 150 ms acquired with a 2.2 ms echo time and 55^{o} excitation flip angle[62]. All SPGR scans were performed using a 18 kHz bandwidth, 12x6 cm^2 field of view, 256 x 128 matrix for the MT-prepared and non-MT-prepared scans and 128 x 64 matrix for the AFI scans, 3 mm slice thickness, and 32 slices. One additional MT-prepared SPGR scan was performed using the same imaging parameters except for a 250 kHz offset frequency and 500° flip angle for negligible MT effect. Total scan time for the mCRI protocol was 90 minutes.

MR Examination

An MR examination of a bovine ex-vivo sample was performed using a 3.0T scanner (Discovery MR750, GE Healthcare, Waukesha, WI) and an 8-channel phased-array extremity coil (In Vivo, Orlando, FL). This examination consisted of the following sequences: 1) the mCRI protocol described in the previous section, and 2) an SPGR sequence with iterative decomposition of water and fat with echo asymmetry and least-squares estimation (IDEAL) fat-water separation[73] acquired using a 12.4 ms repetition time, 3.4 ms, 4.2 ms, and 5.0 ms echo times, 14^{o} excitation

flip angle, 31 kHz bandwidth, 12x9 cm^2 field of view, 256 x 192 matrix, 32 slices, 3 mm slice thickness, and one signal average.

Cartilage qMT Parameter Map Reconstruction

Quantitative MR parameter maps of patellar cartilage were reconstructed using in-house software developed in MATLAB (MATLAB 2011b, MathWorks Inc, Natick, MA). The MT-prepared and non-MT-prepared SPGR datasets were simultaneously fitted on a pixel-by-pixel basis using a non-linear least squares two-pool model to create cartilage f, k and T_2^B maps[56]. Both excitation flip angle and MT saturation power were corrected for each pixel using the flip angle maps acquired from the AFI scans.

4.3 Results

Figures 4-4 and **4-5** show f, k, and T_2^B parametric maps obtained with and without MT differencing.

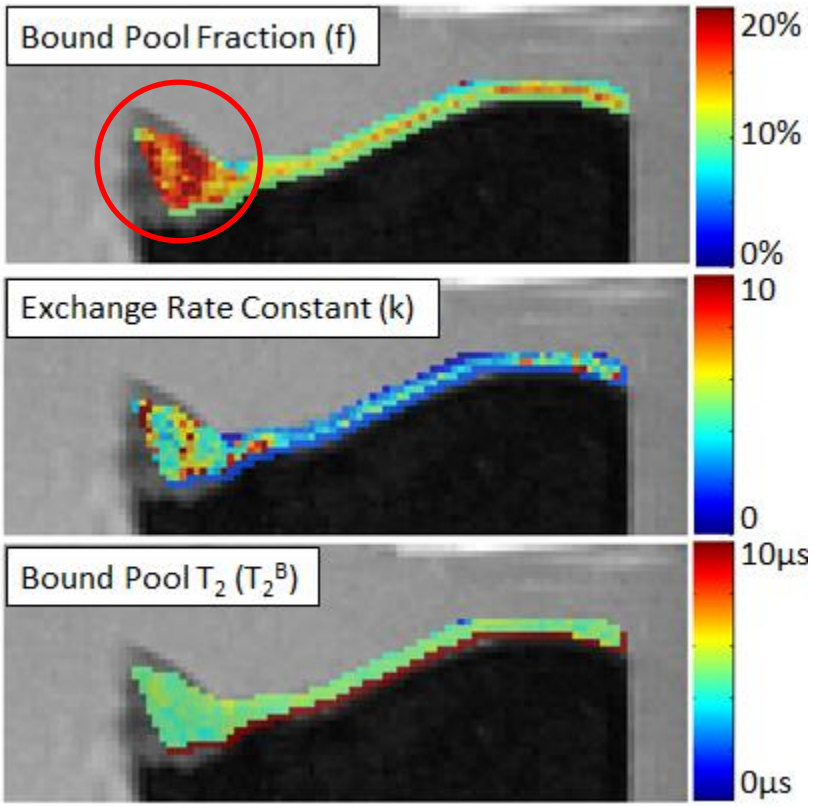

Figure 4-6. f, k, and T_2^B parametric maps obtained without MT differencing. The circled area corresponds to tendon, which has higher bound pool fraction and possibly higher exchange rate constant than cartilage. The difference in macromolecular content and structure, as well as changes in hydration, may account for these parametric differences.

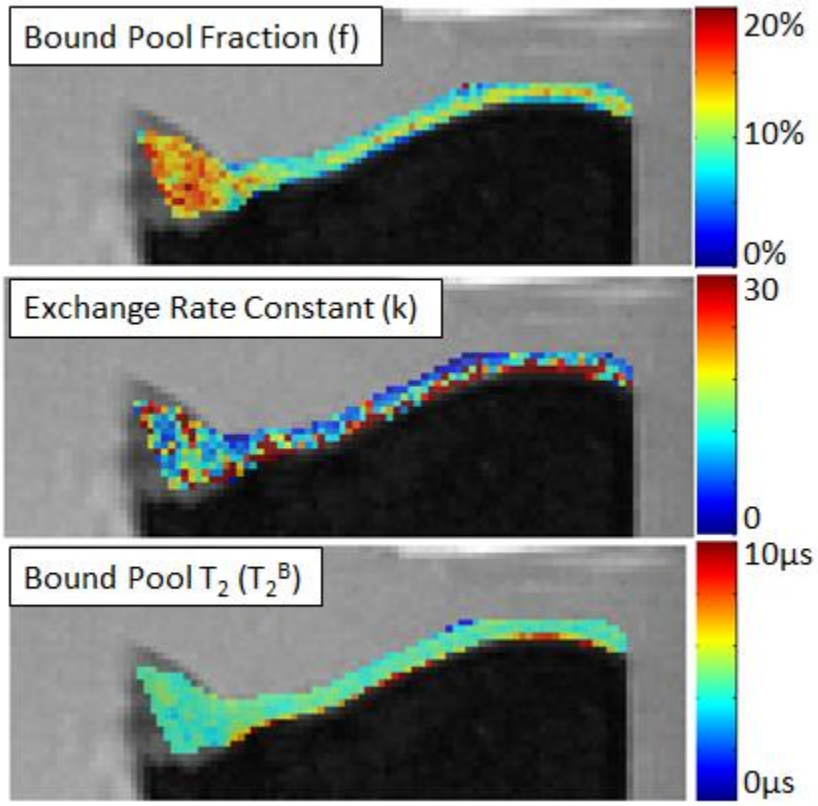

Figure 4-7. f, k, and T_2^B parametric maps obtained with MT differencing. Bound pool fraction (f) appears decreased compared to f obtained without MT differencing. Exchange rate constant (k) is noticeably noisier, which is expected since the differencing operation provides a tradeoff between more noise and suppressed artifacts from non-exchanging signals. T_2^B near the tide mark shows less errors compared to the T_2^B obtained without differencing.

Figures 4-6 and **4-7** show f, k, and T_2^B parametric maps obtained with and without magnetization transfer differencing. Parametric maps with MT differencing show lower f values in both tendon and cartilage, and decreased errors near the tidemark for T_2^B. However, there is

noticeably more noise in the k maps. This is understandable, since taking the difference of two signals introduces more noise and therefore decreases the SNR.

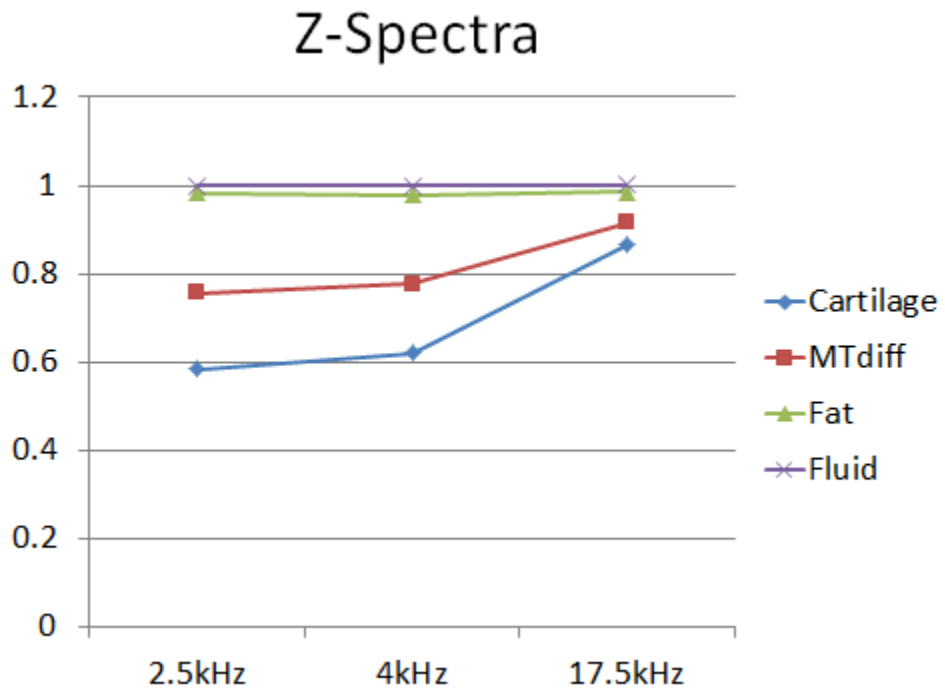

Figure 4-8. Z-spectra of the cartilage, fluid, and fat signals, including the corrected cartilage signal after MT differencing. The corrected cartilage signal shows less saturation than the apparent cartilage signal, possibly due to out-of-phase destructive interference with fat and H_2O in cartilage-dominant voxels. The decreased saturation explains the decreased bound pool fraction.

Figure 4-8 shows the z-spectra of the cartilage, fluid, and fat signals. The cartilage signal is shown before differencing (blue) and after MT differencing (red). After differencing, the corrected cartilage signal suggests less saturation compared to the apparent cartilage signal.

4.4 Conclusions

qMT parametric maps for ex-vivo cartilage have acceptable image quality and can differentiate different tissues. Bound pool fraction was visibly higher and exchange rate constant slightly higher for tendon compared to patellar cartilage. The parameters seem to fall within similar ranges compared to qMT parameters for in-vivo cartilage.

qMT parametric maps obtained through MT differenced signal yielded small but significant differences compared to without MT differencing. In particular, bound pool fraction (f) was visibly lower, and the error at the tide mark for T_2^B visibly disappeared after differencing. However, the increased noise due to signal differencing also decreased SNR, resulting in a slightly noisier k map. Regardless, MT differencing is a useful tool that only requires the addition of an MT-prepared acquisition with negligible MT effect ($\mathbf{MT_{OFF}}$).

Ex-vivo qMT analysis requires further work. Ex-vivo imaging studies are most useful in understanding the biological significance in the context of changes in the image parameters. Degradation studies, where ex-vivo cartilage is treated with collagenase or trypsin and imaged before and after treatment, can help to explain how qMT parameters directly relate to macromolecular content and ultra-structural changes in cartilage. We previously investigated qMT parametric changes due to cartilage degradation in a small study with one sample before and after trypsin treatment, but more samples will be needed to further validate our preliminary findings. We also previously investigated collagen before and after thermal denaturation, to

assess purely ultra-structural changes and the relationship to changes in qMT parameters, but again this was performed with a small number of samples.

The magic angle effect for qMT imaging in cartilage remains largely unknown. We briefly investigated qMT parameters in the saggital plane of the knee in an in-vivo scan, and found an absence of the magic angle effect in T_2^B (See **Chapter 2**). However, further investigation will be necessary, and ex-vivo imaging seems promising to formally investigate the magic angle effect.

This study demonstrates the feasibility in performing robust qMT imaging studies for ex-vivo analysis. Regardless, further imaging developments for qMT may expand the range of possibilities for ex-vivo studies. Acceleration techniques for qMT imaging can enable ex-vivo studies to increase both in-plane and through-plane resolution within the same imaging time. Other quantitative models for qMT imaging may also observe additional properties, such as modelling a non-exchanging pool to separate and investigate non-exchanging species, or simultaneously observing qMT and multi-component relaxation parameters.

Chapter 5: A Compressed Sensing Strategy for Accelerating MSK qMT Applications

Despite the relative time efficiency of mCRI imaging and recent developments in protocol optimization, musculoskeletal imaging demands high in-plane resolution which sometimes requires tradeoffs in slice thickness, SNR, or coverage. Previous mCRI in-vivo studies have been limited to the patellofemoral joint of the knee, or limited coverage of the knee in the saggital plane [64,68,85,87,88]. Acceleration techniques may be useful in recovering SNR when increasing coverage while keeping acquisitions within a reasonable scan time.

This chapter serves to describe a compressed sensing strategy to accelerate qMT imaging for musculoskeletal applications, specifically imaging environments that contain many non-exchanging species (such as fat). MT images may be sparsified, and so a compressed sensing strategy is proposed based off of MT sparsification. The strategy is validated in simulations and also demonstrated on real in-vivo data.

5.1 Introduction

Quantitative magnetization transfer (qMT) imaging based on a two-pool model of MT exchange has been shown to detect early changes in cartilage due to degenerative joint disease[79] and promises to provide a multi-parametric tool for assessment of cartilage status in OA disease[87]. However, qMT requires multiple MT-weighted acquisitions to fit for the two-pool model

parameters, which leads to relatively long acquisition protocols (~30 min) for the musculoskeletal clinical applications even for limited anatomical coverage[64,85]. While parallel imaging acceleration is readily available, it typically results in substantial SNR loss at higher acceleration factors due to g-factor noise amplification.

Recent studies of magnetization transfer networks in tissues suggest that off-resonance MT saturation applied far enough from on-resonance (>2.5 kHz) to avoid direct saturation will have no detectable effect on the fat signal because of the absence of magnetization transfer from fat to water or to protein and membrane phospholipid protons[89(p201)]. This phenomenon was previously exploited to yield fat-free images by subtracting fully sampled magnitude images with ($\mathbf{MT_{ON}}$) and without ($\mathbf{MT_{OFF}}$) saturation[90].

In this work, I propose to utilize the insensitivity of the fat signal to MT saturation to design a novel approach to regularize parallel MRI reconstruction in qMT applications requiring acquisition of multiple MT-weighted measurements.

5.2 Theory

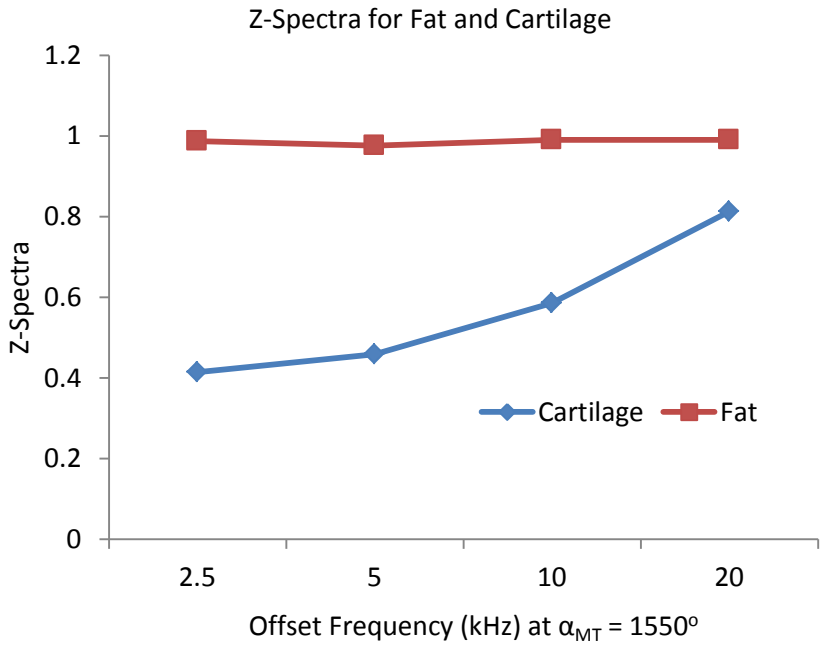

Figure 5-1. An example Z-spectra of the human knee for fat and cartilage tissue. Notice that the z-spectra is relatively constant and flat for the fat tissue, since it does not exhibit significant MT effect at 2.5kHz or greater where saturation from the free pool is negligible.

Figure 5-1 shows typical Z-spectra for cartilage and fatty tissues in human knee, which illustrates that the fat signal is not affected by MT pulse at far enough from resonance. As the knee is comprised of large amount of fatty tissues, the result of subtraction of two images with different or no MT weightings exhibit substantial degree of spatial sparsity (**Figure 5-2**).

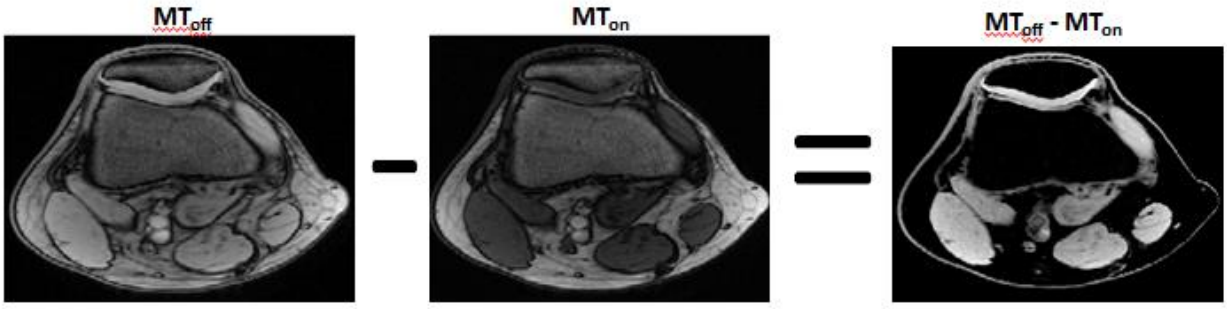

Figure 5-2. Sparsification of the MT-weighted signal. Fat does not exhibit a significant MT effect at high enough offset frequencies (>2.5kHz), and so the subtraction between an MT-weighted signal and a signal without MT weighting can result in a substantial degree of spatial sparsity. Here, fat is largely suppressed, showing signal from cartilage, muscle, blood vessels, and skin.

We hypothesize that such inherent sparsity of MT image differences can be exploited to regularize parallel MRI reconstruction by solving the reconstruction problem, in which the (sparse) difference between reconstruction target and the reference image is penalized by robust/CS-like L1 norm:

$$\mathbf{f}_i = \arg\min_{\mathbf{f}_i} \left(\left\| \mathbf{E}\mathbf{f}_i - \mathbf{d}_i \right\|_2 + \lambda \left\| \mathbf{f}_i - \mathbf{f}_{ref} \right\|_1 \right)$$

Here, $\mathbf{f}_i$ is the i^{th} MT-weighted image (also referred to here as $\mathbf{MT_{on}}$), $\mathbf{f}_{ref}$ is the fully sampled image with the same acquisition pulse sequence but with no MT weighting (also referred to here

as $\mathbf{MT_{off}}$), $\mathbf{E}$ is the encoding matrix comprised of Fourier coefficients and coil sensitivity terms, $\mathbf{d}_i$ is the *k*-space data from all coils, and λ is the regularization parameter.

5.3 Methods

In-vivo 2D Radial Undersampling Study

MT-CS method was compared in one in-vivo case, where the fully sampled dataset was retrospectively undersampled using a 2D radial trajectory with uniform sampling for an acceleration factor of 5. The parameters of in vivo scan were as follows: 8 SPGR data with ($\mathbf{MT_{on}}$) and 1 without ($\mathbf{MT_{off}}$) MT saturation, with TR/TE=42/3.2ms, tm=18ms, α=13°, with 140x140x40mm FOV and 256 x 256 x 10 matrix. $\mathbf{MT_{on}}$ data was acquired at offset frequencies and flip angles 2kHz/1550°, 20kHz/1550°, 17kHz/1450°, 18kHz/1350°, 2.5kHz/750°, 5kHz/750°, 4kHz/700°, 2.5kHz/600°. In the fully sampled acquisition, the dataset was uniformly sampled at 404 2D radial projections per slice. All undersampled reconstructions used 80 of the 404 evenly spaced projections per slice.

The data was reconstructed in the fully sampled case, and also using four acceleration techniques: SENSE, regularized SENSE, the proposed MT-CS strategy, and lastly using the L2-norm of the difference images. The MT-CS strategy and the L2-norm strategy were both reconstructed using the complex difference between $\mathbf{MT_{off}}$ and $\mathbf{MT_{on}}$.

To compare the acceleration techniques, raw MT-weighted images reconstructed from each technique were assessed both qualitatively and quantitatively. Error maps were calculated by taking the difference of the fully sampled raw MT-weighted images with the raw MT-weighted images of each acceleration technique. The acceleration techniques were further compared by observing the parametric maps side-by-side, calculating the error maps in the same manner as described above, computing the mean ROI values of each parameter within the cartilage tissue, and lastly performing a point-by-point correlational analysis to observe the correlation strength between parametric maps from fully sampled images to parametric maps from each acceleration technique.

Digital Phantom Study

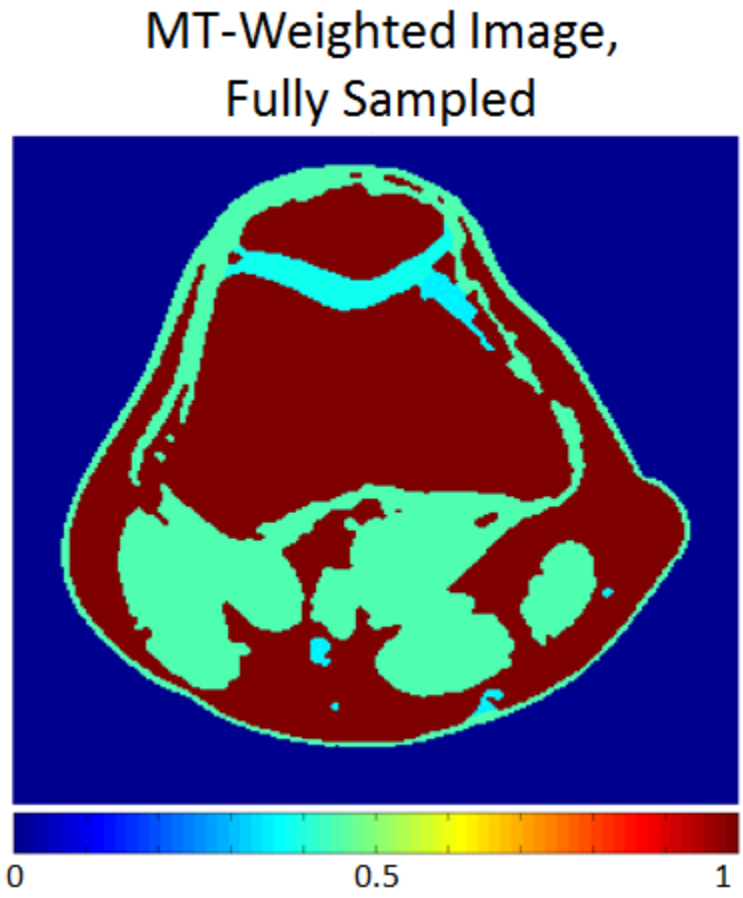

Figure 5-3. Example of an MT-weighted image from the digital phantom used for g-factor analysis. This particular MT-weighted image is also used for demonstrating the raw image reconstruction with various acceleration techniques in **Figure 5-12**.

A digitally generated knee phantom containing fat, cartilage and muscle tissues was generated in the axial plane (**Figure 5-3**) and used to simulate multiple MT points according to the in vivo experiment as described above. Individual simulated MT images were multiplied by 8 separately

measured coils sensitivity profiles and then undersampled using a Poisson disc distribution with a fully sampled center of k-space with varying undersampling for an effective acceleration factor of 6. Monte-Carlo simulations were run by adding white complex value Gaussian noise to the datasets. The minimization problem was solved using iteratively reweighted least squares approach[91]. The proposed strategy was compared to images and estimated parametric maps generated by SENSE without and with L1 regularization on the image itself (referred to as regularized SENSE), which corresponds to zero-valued reference image.

For this study, g-factor analysis involved comparing the mean, standard deviation, and bias images for each acceleration technique.

5.4 Results

Figure 5-4 illustrates the image quality reconstructed by MT-CS, L2-norm, regularized SENSE, and SENSE approaches.

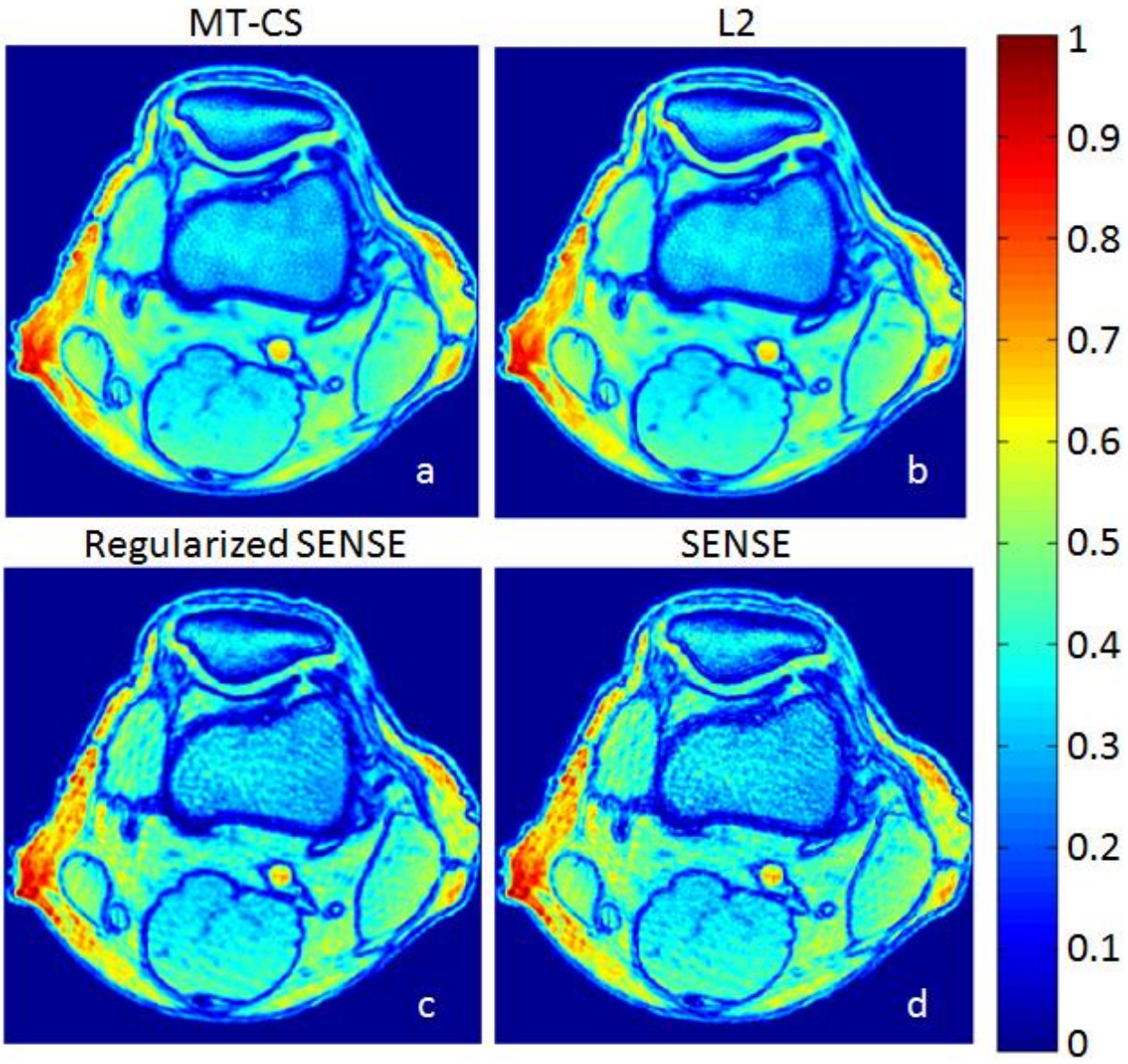

Figure 5-4. Raw in-vivo images for an MT-weighted image using different acceleration strategies, with 5X acceleration using a 2D radial sequence with a uniform sampling pattern.

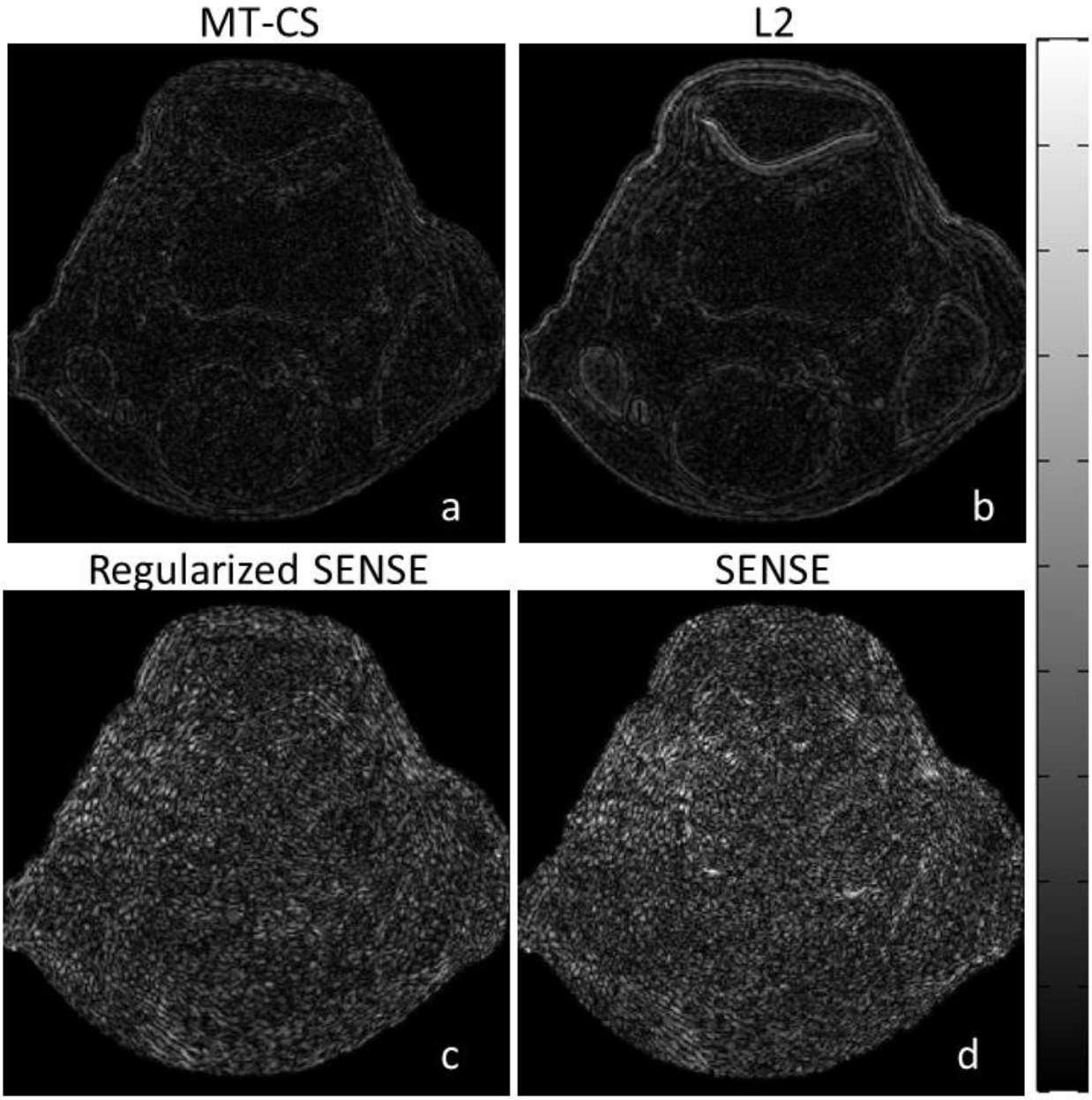

Figure 5-5. Error maps of raw in-vivo data for an MT-weighted image, with 5X acceleration using a 2D radial sequence with a uniform sampling pattern. Error maps were generated by taking the difference between fully sampled image and various acceleration techniques. Error here is amplified 5X. Compared with all four acceleration techniques, our proposed strategy as shown in **(a)** demonstrates

the least error with minimal structural defects. In contrast, the error in the L2 image **(b)** noticeably reveals structure along the cartilage. Lastly, the error is noticeably high for both the regularized SENSE **(c)** and SENSE **(d)** images.

Figure 5-5 illustrates the error propagation of the raw images reconstructed by MT-CS, L2, SENSE, and regularized SENSE approaches. Note the reduced error in the imaging plane for MT-CS and L2 images compared to SENSE and regularized SENSE. However, L2 regularization introduces structured bias into the resulting image.

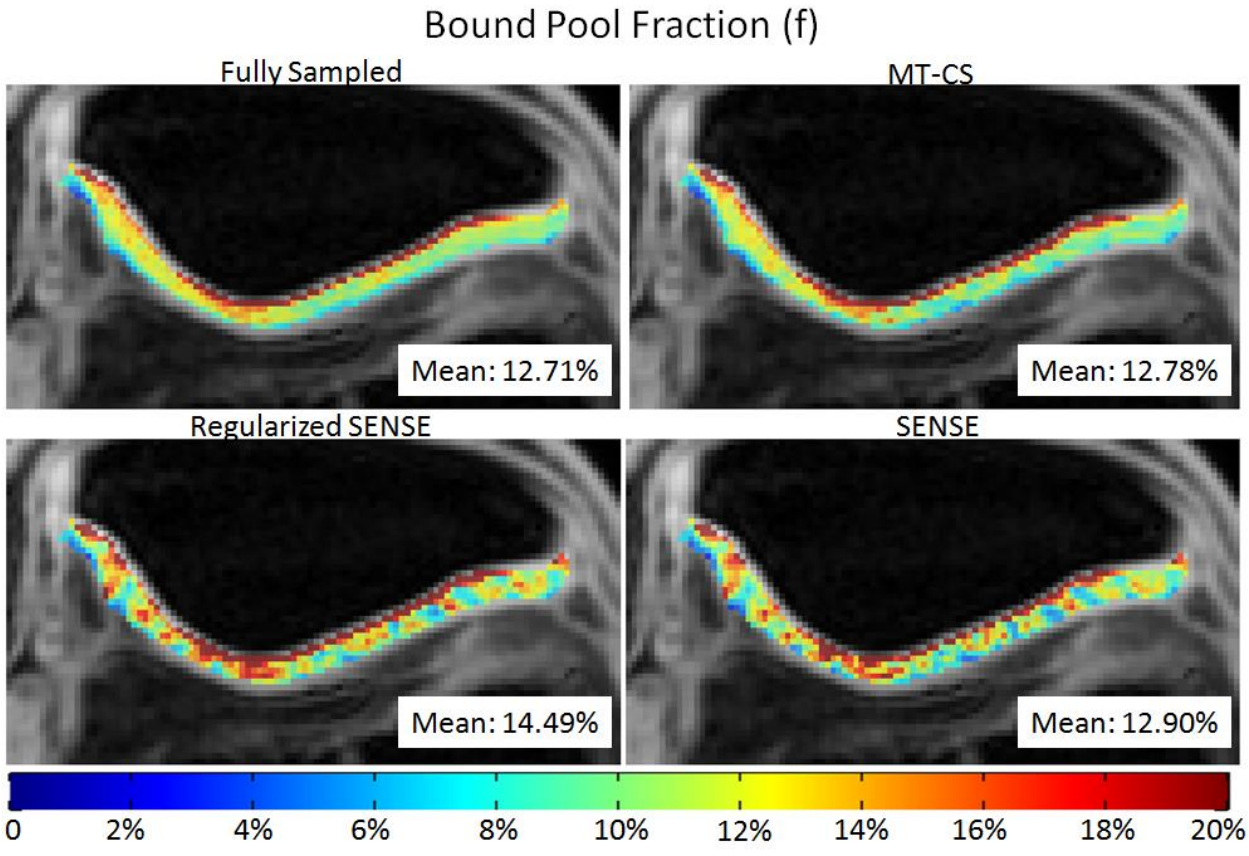

Figure 5-6. Bound pool fraction (f) parametric maps between fully sampled images and accelerated images at 5X acceleration with uniform 2D radial undersampling. Mean ROI values for each reconstruction technique are also shown for comparison. Note that the bound pool fraction as calculated with the MT-CS technique most qualitatively matches the bound pool fraction calculated from fully sampled images. The mean ROI value for bound pool fraction as calculated by the regularized SENSE technique is noticeably higher than the mean ROI value for bound pool fraction from fully sampled images. While SENSE has a similar mean ROI value, there are clear locally regional differences compared to the fully sampled case.

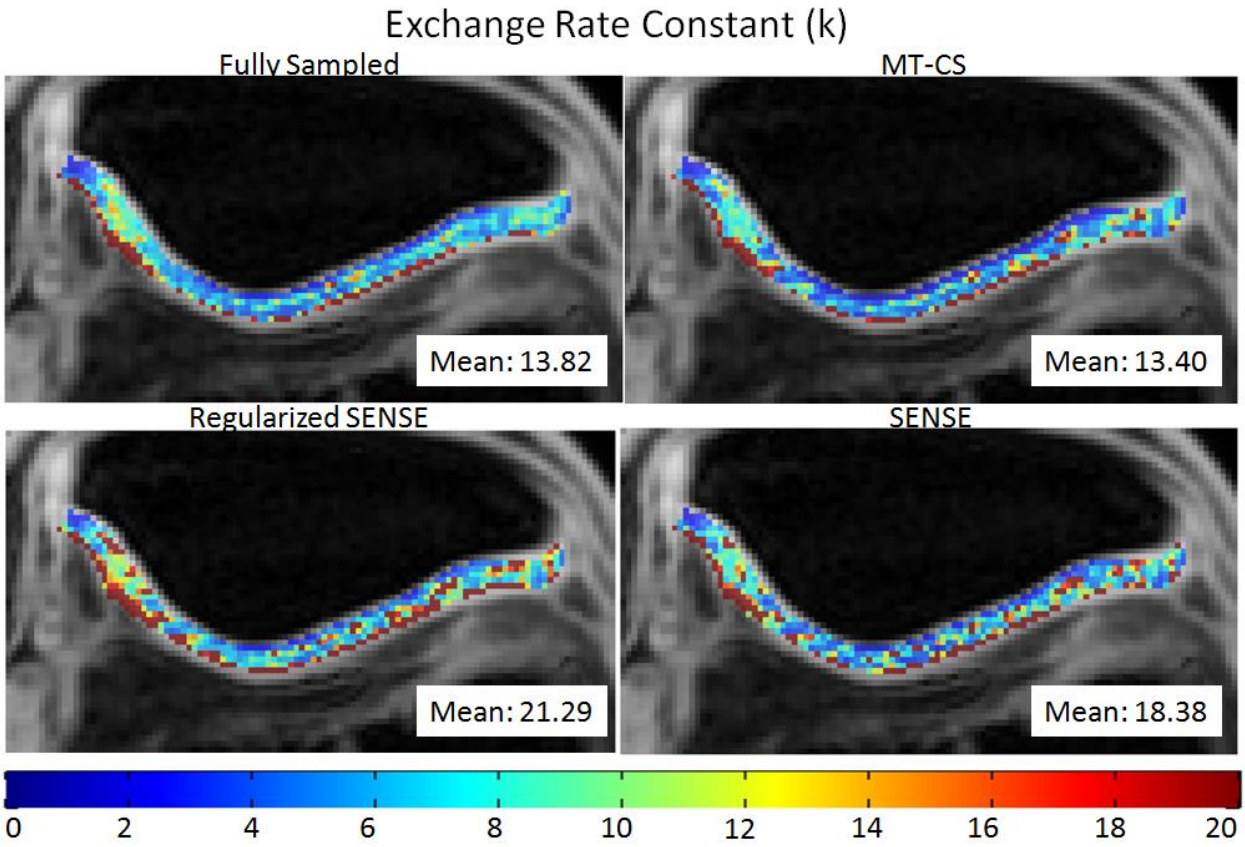

Figure 5-7. Exchange rate constant (k) parametric maps between fully sampled images and accelerated images at 5X acceleration with uniform 2D radial undersampling. Mean ROI values for each reconstruction technique are also shown for comparison. In all cases, exchange rate constant is noisy (consistent with the literature), but MT-CS shows the fewest outliers compared to SENSE and regularized SENSE. The presence of these outliers markedly increases the mean ROI value, which explains the significantly higher mean values for SENSE and regularized SENSE.

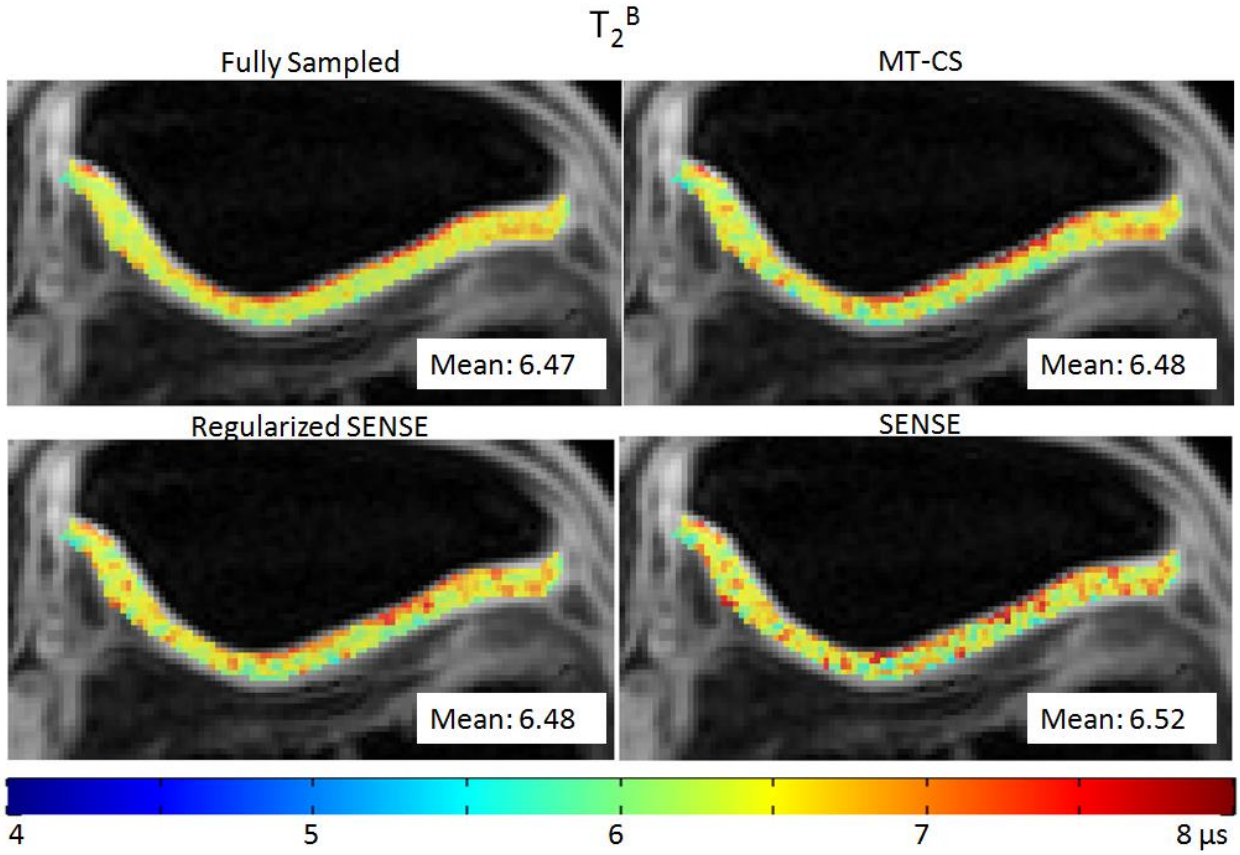

Figure 5-8. Bound pool T_2 (T_2^B) parametric maps between fully sampled images and accelerated images at 5X acceleration with uniform 2D radial undersampling. Mean ROI values for each reconstruction technique are also shown for comparison. In all cases, mean ROI values seem very similar between acceleration techniques. However, T_2^B maps for SENSE appear slightly noisier compared to the other acceleration techniques.

Figures 5-6, **5-7**, and **5-8** show the f, k, and T_2^B parametric maps obtained from the fully sampled case vs. the accelerated images. Mean ROI values for bound pool fraction (f) maps were 12.71% for the fully sampled case, 12.78% for MT-CS, 14.49% for regularized SENSE, and

12.90% for SENSE. Mean ROI values for exchange rate constant (k) maps were 13.82 for the fully sampled case, 13.40 for MT-CS, 21.29 for Regularized SENSE, and 18.38 for SENSE. Mean ROI values for bound pool T_2 (T_2^B) were 6.47μs for the fully sampled case, 6.48 μs for MT-CS, 6.48 for regularized SENSE, and 6.52 for SENSE.

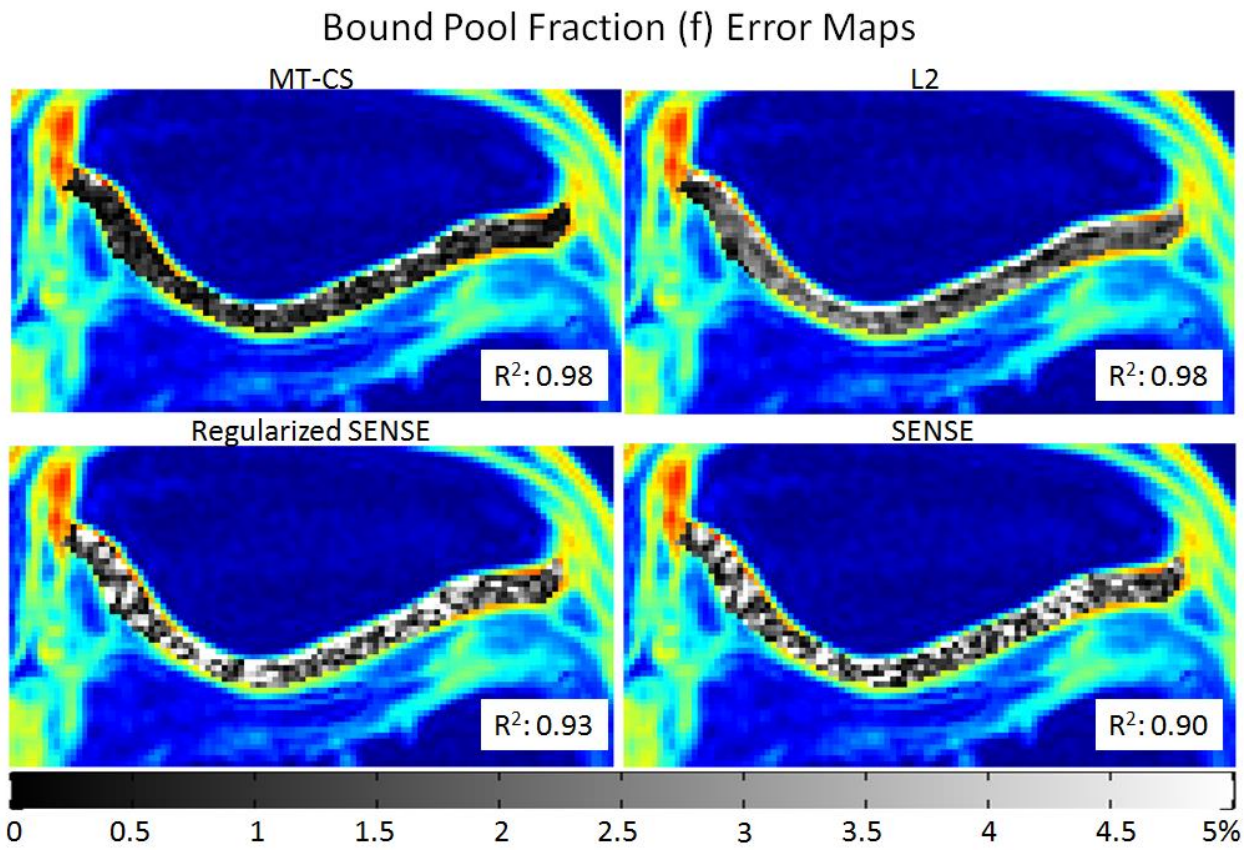

Figure 5-9. Error maps (amplified at 4X) of bound pool fraction (f) between different acceleration techniques at 5X acceleration with uniform 2D radial undersampling. Error maps were generated by taking the difference between the f map from the fully sampled case with the f map of the given acceleration technique. R^2 values are also provided to demonstrate the pixel-by-pixel correlation strength compared to the f values of the fully sampled case. Notice that the f from MT-CS has visibly lower error among all of the other acceleration techniques and a high correlation R^2 value at 0.98.

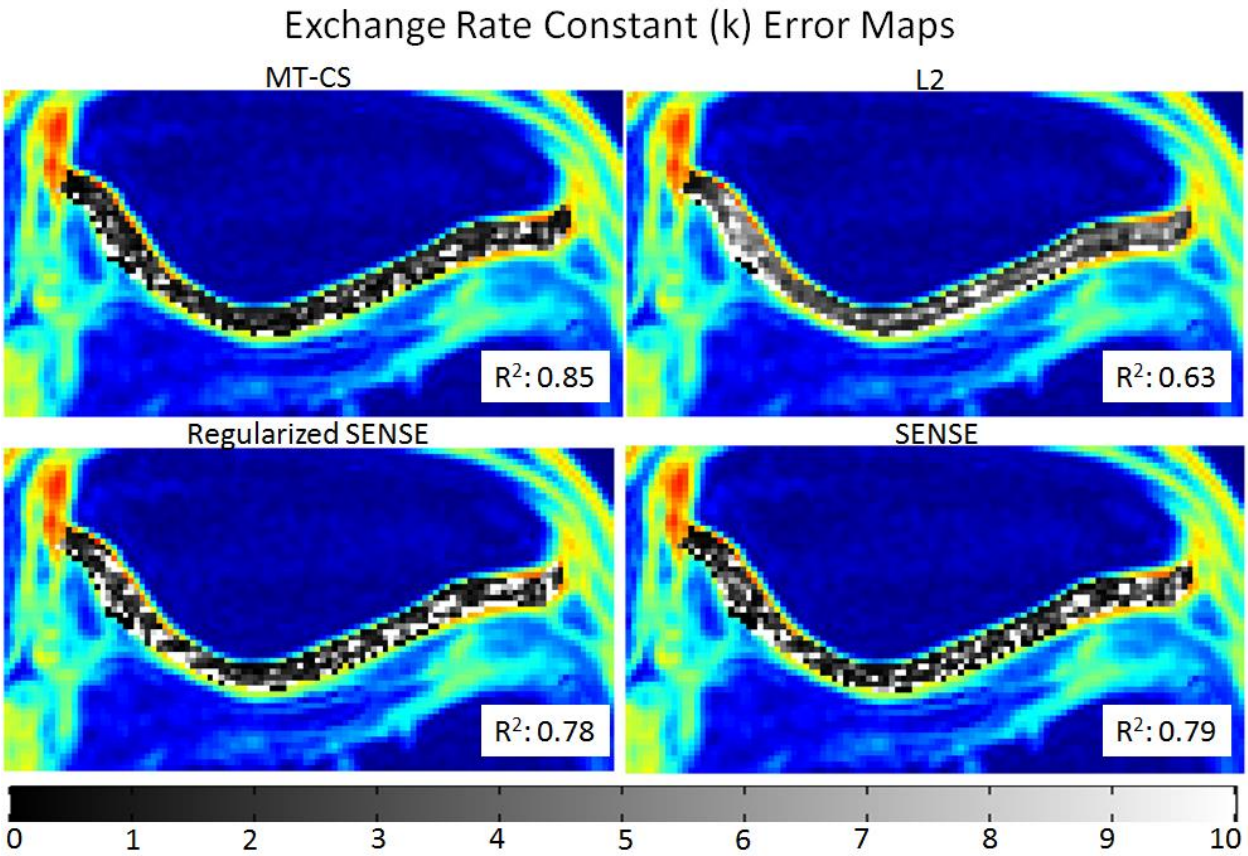

Figure 5-10. Error maps (amplified at 2X) of exchange rate constant (k) between different acceleration techniques at 5X acceleration with uniform 2D radial undersampling. Error maps were generated by taking the difference between the k map from the fully sampled case with the k map of the given acceleration technique. R^2 values are also provided to demonstrate the pixel-by-pixel correlation strength compared to the k values of the fully sampled case. Notice that the k from MT-CS has visibly lower error among all of the other acceleration techniques and a strong correlation R^2 value at 0.85.

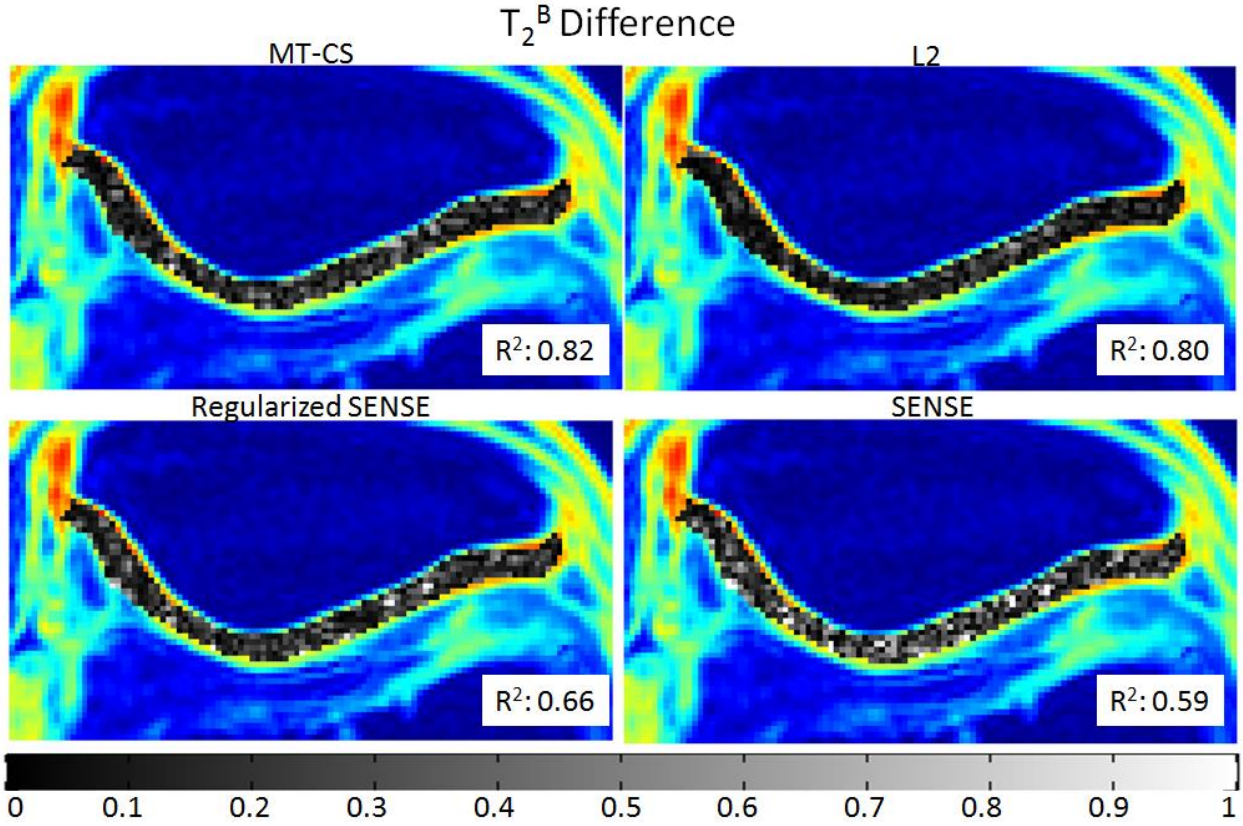

Figure 5-11. Error maps (amplified at 84X) of bound pool T_2 (T_2^B) between different acceleration techniques at 5X acceleration with uniform 2D radial undersampling. Error maps were generated by taking the difference between the T_2^B map from the fully sampled case with the T_2^B map of the given acceleration technique. R^2 values are also provided to demonstrate the pixel-by-pixel correlation strength compared to the T_2^B values of the fully sampled case. Notice that the T_2^B from MT-CS has visibly lower error than the T_2^B maps from SENSE and regularized SENSE and a strong correlation R^2 value at 0.82.

Figure 5-9, **5-10**, and **5-11** illustrate the error propagation from accelerated images to f, k, and T_2^B maps. Point-by-point correlation analysis between the fully sampled case and each acceleration technique is shown for each parameter. R^2 values for bound pool fraction (f) were 0.98 for MT-CS, 0.98 for L2, 0.93 for regularized SENSE, and 0.90 for SENSE. R^2 values for exchange rate constant (k) were 0.85 for MT-CS, 0.63 for L2, 0.78 for regularized SENSE, and 0.79 for SENSE. R^2 values for bound pool T_2 (T_2^B) were 0.82 for MT-CS, 0.80 for L2, 0.66 for regularized SENSE, and 0.59 for SENSE.

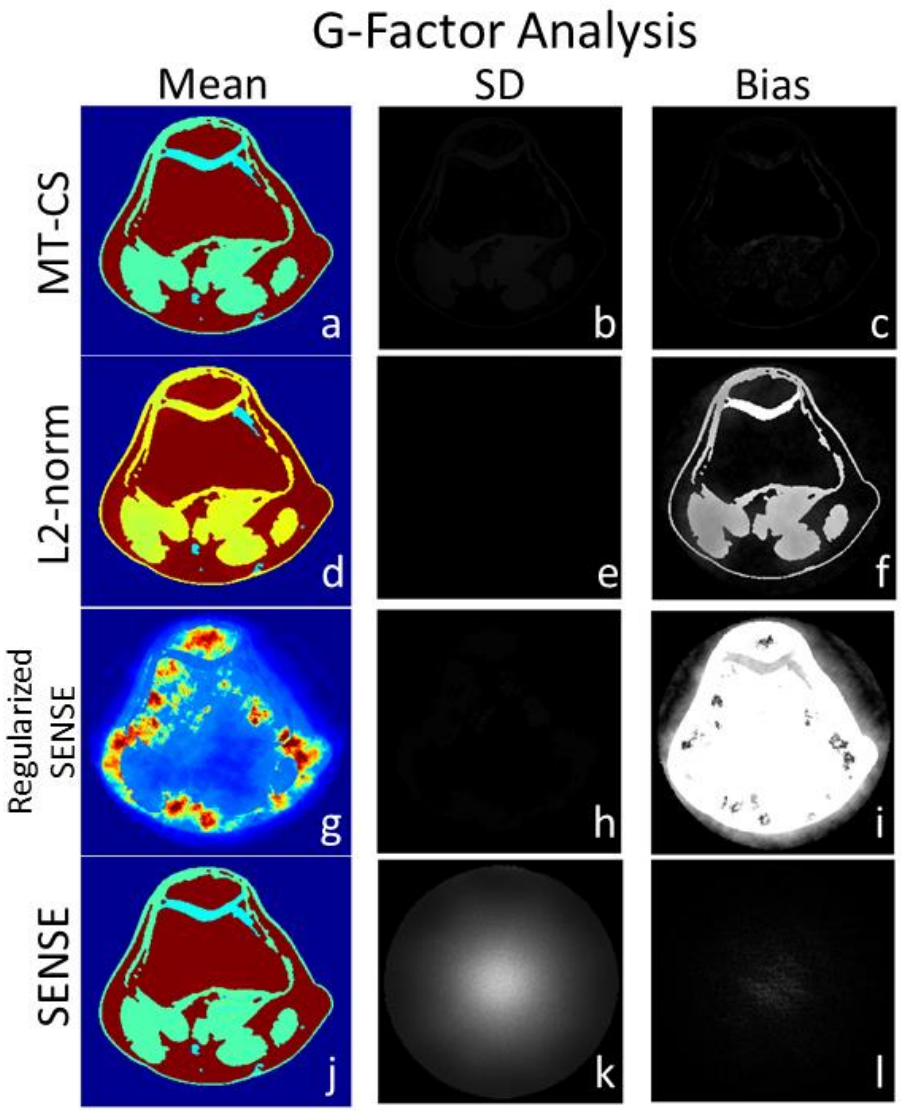

Figure 5-12. Digital simulation g-factor analysis of raw images from various acceleration techniques. The mean images for MT-CS (a) and SENSE (j) closely resemble the fully sampled digital phantom from **Figure 5-3**. However, the standard deviation from SENSE reconstruction is noticeably high. In contrast, MT-CS seems to provide the best tradeoff in terms of the standard deviation (b) and bias (c).

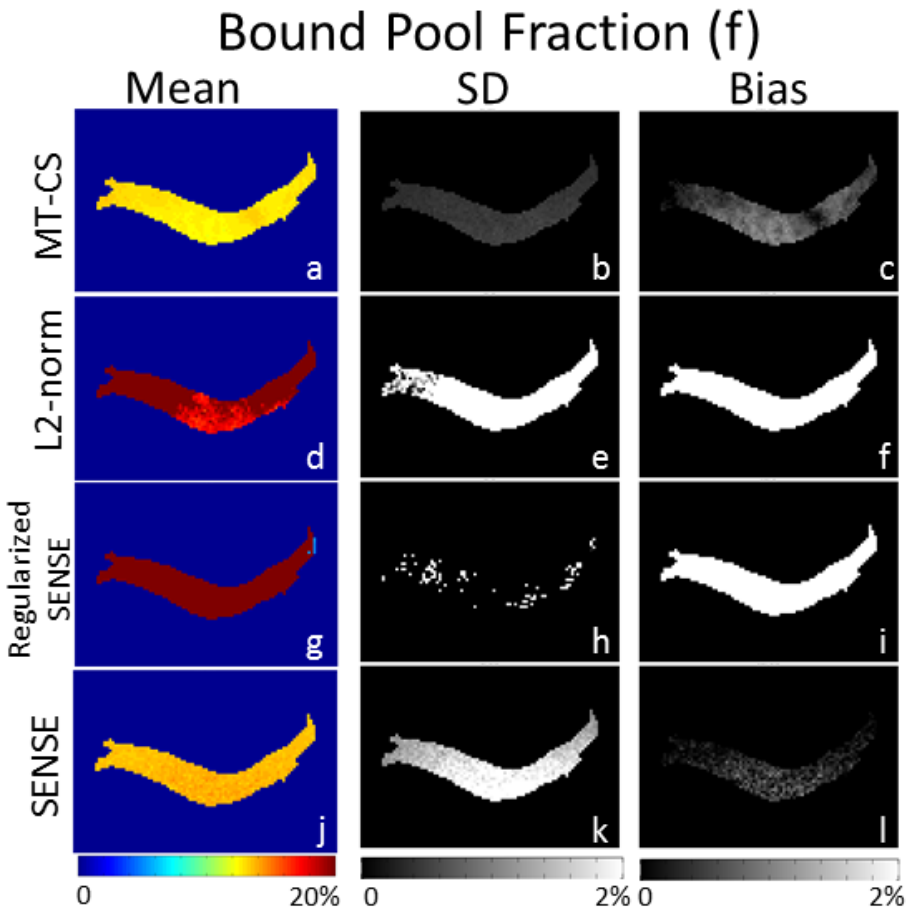

Figure 5-13. g-factor analysis of bound pool fraction (f) parametric maps between different acceleration approaches. f maps from MT-CS (a-c) provide the closest approximation to the f maps from fully sampled images, with low standard deviation (b) and bias (c). f maps from SENSE (j-l) provide even lower bias (l), but suffer from high standard deviation (k).

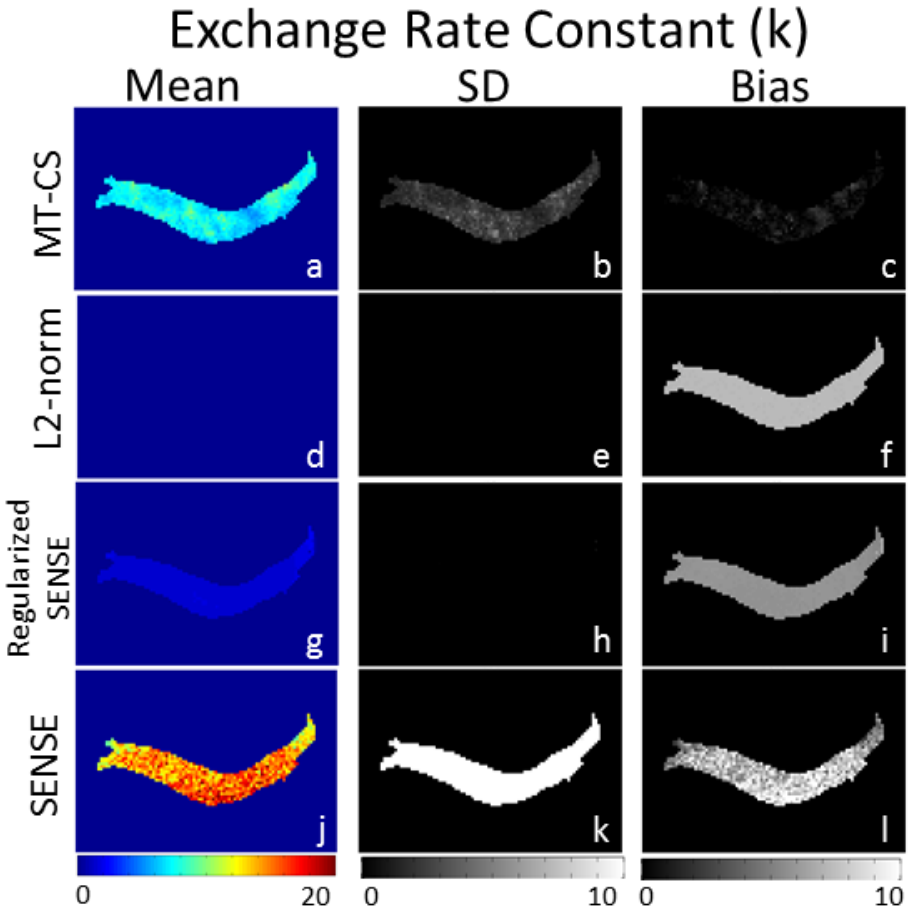

Figure 5-14. g-factor analysis of exchange rate constant (k) parametric maps between different acceleration approaches. By far, k maps from MT-CS (a-c) provide the closest approximation to the k maps from fully sampled images, with low standard deviation (b) and bias (c). The other regularized approaches (d-f, g-i) provide very low standard deviation (e, h) in k maps, but the high bias (f, i) suggests over-constrained reconstruction.

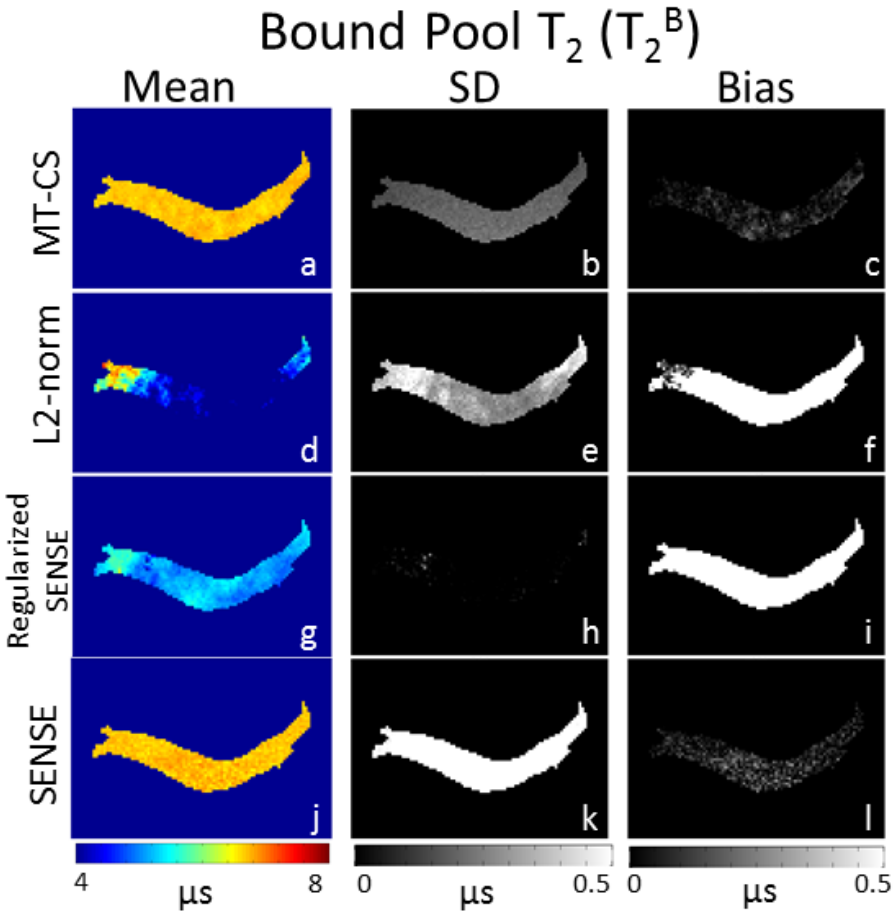

Figure 5-14. g-factor analysis of bound pool T_2 (T_2^B) parametric maps between different acceleration approaches. T_2^B maps from MT-CS (a-c) provide the closest approximation to the T_2^B maps from fully sampled images, with relatively low standard deviation and bias. Regularized SENSE (g-i) provides lower standard deviation (h) but significantly higher bias (i). SENSE (j-l) also provides a close approximation of T_2^B as seem from the low bias (l), but has high standard deviation (k).

Figure 5-11, 5-12, 5-13, and 5-14 shows the results of the g-factor analysis from digital phantom simulations. MT-CS seems to provide the best tradeoff in terms of standard deviation and bias for raw MT-weighted reconstructions and all qMT parametric maps (f, k, T_2^B).

5.5 Conclusion

In this work, we proposed a compressed sensing (CS) strategy that exploits unique MT properties of fat to efficiently sparsify the individual MT-weighted measurements by fully sampled reference image. The main requirement is that it should share pulse sequence parameters with the rest of acquisitions except MT saturation ($\mathbf{MT_{OFF}}$), which is typical in qMT methods. In particular, we demonstrated its utility for regularized parallel imaging. Compared to direct application of parallel imaging without and with standard regularization approaches, our proposed MT-CS strategy provides lower noise amplification and bias. As any CS-based technique, our approach was found useful with randomized trajectories, error by exploiting the sparsity of MT subtraction images.

Applying other sparsifying transforms such as wavelets may further enhance this technique. The proposed strategy is likely to have additional ramifications. For example, additional benefits may be expected by utilizing fat-independence in multi-echo acquisitions for improved fat water separations, when a single fat component and multiple MT-weighted water components are estimated jointly from multiple acquired datasets. CS strategy utilizing joint sparsity of MT-weighted water images may further improve acceleration potential of the proposed method. While knee anatomy seems very well-suited to create a sparse environment for recovering MT

signals from undersampled data, this approach could be potentially applied in other anatomies characterized by high level of fatty tissues.

Chapter 6: Summary and Future Work

6.1 Summary

In summary, the goal of this work was to develop non-invasive MRI biomarkers for assessing the content and ultra-structure of the cartilage through qMT. This work addressed multiple aspects of biomarker development, including model selection, protocol optimization, clinical feasibility, ex-vivo protocol development, and acceleration techniques for faster acquisitions.

Because of the attractive tradeoffs in relative time efficiency and accuracy compared to other qMT techniques, modified Cross-Relaxation Imaging (mCRI) was chosen to assess qMT parameters in the knee. Optimization of mCRI protocols involved the selection of MT points from a wide range of offset frequencies and/or flip angles, but brute force search methods may lead to impractical search times. I proposed an iterative voting strategy to search these MT points and intelligently select an appropriate MT combination. These combinations were then demonstrated to provide greater lateral coverage of the in-vivo weight-bearing surfaces of the tibiofemoral joint.

I also demonstrated the feasibility of using CRI to measure the qMT parameters f, k, and T_2^B of the articular cartilage of the knee joint in human subjects. I found significant differences in f and T_2^B of patellar cartilage between asymptomatic volunteers and patients with osteoarthritis which indicates that qMT parameters measured using CRI can detect population differences in cartilage degeneration within the human knee joint.

Furthermore, ex-vivo imaging studies will be important to assess the biological significance of mCRI for cartilage. Toward this end, I developed an mCRI protocol for evaluating ex-vivo cartilage at 3.0T for animal models, which can provide robust measurements of f, k, and T_2^B with higher resolution, wider coverage, and higher SNR. The protocol also provides the additional option of removing non-exchanging signals before fitting mCRI parameters, which can correct for some biases due to non-exchanging pools, but at the tradeoff of decreased SNR.

Previous mCRI in-vivo studies have been limited to the patellofemoral joint of the knee, or limited coverage of the knee in the saggital plane. Acceleration techniques may be useful in recovering SNR when increasing coverage while keeping acquisitions within a reasonable scan time. I proposed and investigated a compressed sensing strategy to accelerate qMT imaging for musculoskeletal applications, specifically imaging environments that contain many non-exchanging species (such as fat). MT images may be sparsified, and so a compressed sensing strategy is proposed based off of MT sparsification. The strategy is validated in simulations and also demonstrated on real in-vivo data.

6.2 Future Work

Many possibilities remain for further investigating qMT parameters in cartilage. A summary of possible future work is detailed below.

6.2.1 Biological Significance

The biological significance of mCRI parameters is still largely unexplored. One previous study has investigated CRI of articular cartilage which measured f and k in ex-vivo human cadaveric cartilage specimens using a two-pool model that fixed T_2^{B} [55]. However, I found statistically significant differences in T_2^{B} between healthy volunteers and patients with osteoarthritis. Additionally, while the previous study has been monumental in motivating this work, the previous study observed macromolecular content by observing only their correlations with CRI parameters and biochemistry. The study was limited in its ability to consider causes for changes in qMT parameters.

Degradation studies, where ex-vivo cartilage is treated with collagenase or trypsin and imaged before and after treatment, can help to explain how qMT parameters directly relate to macromolecular content and ultra-structural changes in cartilage. We previously investigated qMT parametric changes due to cartilage degradation in a small study with one sample before and after trypsin treatment, but more samples will be needed to further validate our preliminary findings. We also previously investigated collagen before and after thermal denaturation, to assess purely ultra-structural changes and the relationship to changes in qMT parameters, but again this was performed with a small number of samples.

The magic angle effect for qMT imaging in cartilage remains largely unknown. We briefly investigated qMT parameters in the saggital plane of the knee in an in-vivo scan, and found an

absence of the magic angle effect in T_2^B (See **Chapter 2**). However, further investigation will be necessary, and ex-vivo imaging seems promising to formally investigate the magic angle effect.

6.2.2 Whole Knee Protocol Development

Whole knee imaging is crucial for observing all articular cartilage surfaces of the knee, especially since cartilage degeneration occurs frequently nearby the weight-bearing surfaces of the knee. Previous in-vivo cartilage studies in mCRI investigated the patellofemoral joint and also investigated using an optimal selection of MT points to allow for greater coverage of the knee (specifically, the weight-bearing portions of the tibiofemoral interface).

Methods to accelerate mCRI protocols for musculoskeletal applications will be necessary to enable whole knee joint imaging. I proposed and investigated a compressed sensing strategy that can enable at least 5X acceleration. The strategy was shown to correlate highly with parameters calculated from fully sampled images and outperformed conventional acceleration methods. Methods like these can provide their full potential if used to expand the coverage to image the entire knee.

References

1. Anon. From the Centers for Disease Control and Prevention. Arthritis prevalence and activity limitations--United States, 1990. JAMA: the journal of the American Medical Association. 1994 August 3;272(5):346–347.

2. Felson DT. An update on the pathogenesis and epidemiology of osteoarthritis. Radiologic clinics of North America. 2004 January;42(1):1–9, v.

3. Felson DT, Zhang Y. An update on the epidemiology of knee and hip osteoarthritis with a view to prevention. Arthritis and rheumatism. 1998 August;41(8):1343–1355.

4. Lawrence RC, Helmick CG, Arnett FC, Deyo RA, Felson DT, Giannini EH, Heyse SP, Hirsch R, Hochberg MC, Hunder GG, et al. Estimates of the prevalence of arthritis and selected musculoskeletal disorders in the United States. Arthritis and rheumatism. 1998 May;41(5):778–799.

5. Oliveria SA, Felson DT, Reed JI, Cirillo PA, Walker AM. Incidence of symptomatic hand, hip, and knee osteoarthritis among patients in a health maintenance organization. Arthritis and rheumatism. 1995 August;38(8):1134–1141.

6. Burstein D, Bashir A, Gray ML. MRI techniques in early stages of cartilage disease. Investigative Radiology. 2000 October [cited 2011 July 4];35(10):622–638.

7. Chung C, Burdick JA. Engineering cartilage tissue. Advanced Drug Delivery Reviews. 2008 January 14 [cited 2011 July 6];60(2):243–262.

8. Hollander AP, Dickinson SC, Kafienah W. Stem cells and cartilage development: complexities of a simple tissue. Stem Cells (Dayton, Ohio). 2010 November [cited 2011 July 6];28(11):1992–1996.

9. Choi J-A, Gold GE. MR Imaging of Articular Cartilage Physiology. Magnetic Resonance Imaging Clinics of North America. 2011 May [cited 2011 July 4];19(2):249–282.

10. Conway WF, Hayes CW, Loughran T, Totty WG, Griffeth LK, el-Khoury GY, Shellock FG. Cross-sectional imaging of the patellofemoral joint and surrounding structures. Radiographics: A Review Publication of the Radiological Society of North America, Inc. 1991 March [cited 2011 July 6];11(2):195–217.

11. Venn M, Maroudas A. Chemical composition and swelling of normal and osteoarthrotic femoral head cartilage. I. Chemical composition. Annals of the rheumatic diseases. 1977 April;36(2):121–129.

12. Squires GR, Okouneff S, Ionescu M, Poole AR. The pathobiology of focal lesion development in aging human articular cartilage and molecular matrix changes characteristic of osteoarthritis. Arthritis and rheumatism. 2003 May;48(5):1261–1270.

13. Billinghurst RC, Dahlberg L, Ionescu M, Reiner A, Bourne R, Rorabeck C, Mitchell P, Hambor J, Diekmann O, Tschesche H, et al. Enhanced cleavage of type II collagen by collagenases in osteoarthritic articular cartilage. The Journal of clinical investigation. 1997 April 1;99(7):1534–1545.

14. Gold GE, Burstein D, Dardzinski B, Lang P, Boada F, Mosher T. MRI of articular cartilage in OA: novel pulse sequences and compositional/functional markers. Osteoarthritis and cartilage / OARS, Osteoarthritis Research Society. 2006;14 Suppl A:A76–86.

15. Disler DG, McCauley TR, Kelman CG, Fuchs MD, Ratner LM, Wirth CR, Hospodar PP. Fat-suppressed three-dimensional spoiled gradient-echo MR imaging of hyaline cartilage defects in the knee: comparison with standard MR imaging and arthroscopy. AJR. American journal of roentgenology. 1996 July;167(1):127–132.

16. Altman RD. Early management of osteoarthritis. The American journal of managed care. 2010 March;16 Suppl Management:S41–47.

17. Bashir A, Gray ML, Boutin RD, Burstein D. Glycosaminoglycan in articular cartilage: in vivo assessment with delayed Gd(DTPA)(2-)-enhanced MR imaging. Radiology. 1997 November;205(2):551–558.

18. Bashir A, Gray ML, Burstein D. Gd-DTPA2- as a measure of cartilage degradation. Magnetic resonance in medicine: official journal of the Society of Magnetic Resonance in Medicine / Society of Magnetic Resonance in Medicine. 1996 November;36(5):665–673.

19. Borthakur A, Shapiro EM, Beers J, Kudchodkar S, Kneeland JB, Reddy R. Sensitivity of MRI to proteoglycan depletion in cartilage: comparison of sodium and proton MRI. Osteoarthritis and cartilage / OARS, Osteoarthritis Research Society. 2000 July;8(4):288–293.

20. Shapiro EM, Borthakur A, Gougoutas A, Reddy R. 23Na MRI accurately measures fixed charge density in articular cartilage. Magnetic resonance in medicine: official journal of the Society of Magnetic Resonance in Medicine / Society of Magnetic Resonance in Medicine. 2002 February;47(2):284–291.

21. Duvvuri U, Kudchodkar S, Reddy R, Leigh JS. T(1rho) relaxation can assess longitudinal proteoglycan loss from articular cartilage in vitro. Osteoarthritis and cartilage / OARS, Osteoarthritis Research Society. 2002 November;10(11):838–844.

22. Duvvuri U, Reddy R, Patel SD, Kaufman JH, Kneeland JB, Leigh JS. T1rho-relaxation in articular cartilage: effects of enzymatic degradation. Magnetic resonance in medicine: official

journal of the Society of Magnetic Resonance in Medicine / Society of Magnetic Resonance in Medicine. 1997 December;38(6):863–867.

23. Mosher TJ, Dardzinski BJ, Smith MB. Human articular cartilage: influence of aging and early symptomatic degeneration on the spatial variation of T2--preliminary findings at 3 T. Radiology. 2000 January;214(1):259–266.

24. Dardzinski BJ, Mosher TJ, Li S, Van Slyke MA, Smith MB. Spatial variation of T2 in human articular cartilage. Radiology. 1997 November;205(2):546–550.

25. Burstein D, Gray ML, Hartman AL, Gipe R, Foy BD. Diffusion of small solutes in cartilage as measured by nuclear magnetic resonance (NMR) spectroscopy and imaging. Journal of orthopaedic research: official publication of the Orthopaedic Research Society. 1993 July;11(4):465–478.

26. Mlynárik V, Sulzbacher I, Bittsanský M, Fuiko R, Trattnig S. Investigation of apparent diffusion constant as an indicator of early degenerative disease in articular cartilage. Journal of magnetic resonance imaging: JMRI. 2003 April;17(4):440–444.

27. Raya JG, Melkus G, Adam-Neumair S, Dietrich O, Mützel E, Reiser MF, Putz R, Kirsch T, Jakob PM, Glaser C. Diffusion-tensor imaging of human articular cartilage specimens with early signs of cartilage damage. Radiology. 2013 March;266(3):831–841.

28. Gray ML, Burstein D, Lesperance LM, Gehrke L. Magnetization transfer in cartilage and its constituent macromolecules. Magnetic Resonance in Medicine: Official Journal of the Society of Magnetic Resonance in Medicine / Society of Magnetic Resonance in Medicine. 1995 September [cited 2011 July 5];34(3):319–325.

29. Kim DK, Ceckler TL, Hascall VC, Calabro A, Balaban RS. Analysis of water-macromolecule proton magnetization transfer in articular cartilage. Magnetic Resonance in Medicine: Official Journal of the Society of Magnetic Resonance in Medicine / Society of Magnetic Resonance in Medicine. 1993 February [cited 2011 July 5];29(2):211–215.

30. Schmitt B, Zbýn S, Stelzeneder D, Jellus V, Paul D, Lauer L, Bachert P, Trattnig S. Cartilage quality assessment by using glycosaminoglycan chemical exchange saturation transfer and (23)Na MR imaging at 7 T. Radiology. 2011 July;260(1):257–264.

31. Singh A, Haris M, Cai K, Kassey VB, Kogan F, Reddy D, Hariharan H, Reddy R. Chemical exchange saturation transfer magnetic resonance imaging of human knee cartilage at 3 T and 7 T. Magnetic resonance in medicine: official journal of the Society of Magnetic Resonance in Medicine / Society of Magnetic Resonance in Medicine. 2012 August;68(2):588–594.

32. Henkelman RM, Huang X, Xiang QS, Stanisz GJ, Swanson SD, Bronskill MJ. Quantitative interpretation of magnetization transfer. Magnetic Resonance in Medicine: Official Journal of the

Society of Magnetic Resonance in Medicine / Society of Magnetic Resonance in Medicine. 1993 June [cited 2011 July 5];29(6):759–766.

33. Sled JG, Levesque I, Santos AC, Francis SJ, Narayanan S, Brass SD, Arnold DL, Pike GB. Regional variations in normal brain shown by quantitative magnetization transfer imaging. Magnetic resonance in medicine: official journal of the Society of Magnetic Resonance in Medicine / Society of Magnetic Resonance in Medicine. 2004 February;51(2):299–303.

34. Yarnykh VL. Pulsed Z-spectroscopic imaging of cross-relaxation parameters in tissues for human MRI: theory and clinical applications. Magnetic Resonance in Medicine: Official Journal of the Society of Magnetic Resonance in Medicine / Society of Magnetic Resonance in Medicine. 2002 May [cited 2011 July 5];47(5):929–939.

35. Henkelman RM, Stanisz GJ, Menezes N, Burstein D. Can MTR be used to assess cartilage in the presence of Gd-DTPA2-? Magnetic Resonance in Medicine: Official Journal of the Society of Magnetic Resonance in Medicine / Society of Magnetic Resonance in Medicine. 2002 December [cited 2011 September 5];48(6):1081–1084.

36. Li W, Hong L, Hu L, Magin RL. Magnetization transfer imaging provides a quantitative measure of chondrogenic differentiation and tissue development. Tissue Engineering. Part C, Methods. 2010 December [cited 2011 November 9];16(6):1407–1415.

37. Stanisz GJ, Odrobina EE, Pun J, Escaravage M, Graham SJ, Bronskill MJ, Henkelman RM. T1, T2 relaxation and magnetization transfer in tissue at 3T. Magnetic Resonance in Medicine: Official Journal of the Society of Magnetic Resonance in Medicine / Society of Magnetic Resonance in Medicine. 2005 September [cited 2011 July 5];54(3):507–512.

38. Rizkalla G, Reiner A, Bogoch E, Poole AR. Studies of the articular cartilage proteoglycan aggrecan in health and osteoarthritis. Evidence for molecular heterogeneity and extensive molecular changes in disease. The Journal of clinical investigation. 1992 December;90(6):2268–2277.

39. Reiter DA, Lin P-C, Fishbein KW, Spencer RG. Multicomponent T2 relaxation analysis in cartilage. Magnetic resonance in medicine: official journal of the Society of Magnetic Resonance in Medicine / Society of Magnetic Resonance in Medicine. 2009 April;61(4):803–809.

40. Reiter DA, Roque RA, Lin P-C, Irrechukwu O, Doty S, Longo DL, Pleshko N, Spencer RG. Mapping proteoglycan-bound water in cartilage: Improved specificity of matrix assessment using multiexponential transverse relaxation analysis. Magnetic resonance in medicine: official journal of the Society of Magnetic Resonance in Medicine / Society of Magnetic Resonance in Medicine. 2011 February;65(2):377–384.

41. Reiter DA, Roque RA, Lin P-C, Doty SB, Pleshko N, Spencer RG. Improved specificity of cartilage matrix evaluation using multiexponential transverse relaxation analysis applied to pathomimetically degraded cartilage. NMR in biomedicine. 2011 December;24(10):1286–1294.

42. Poole AR, Kobayashi M, Yasuda T, Laverty S, Mwale F, Kojima T, Sakai T, Wahl C, El-Maadawy S, Webb G, et al. Type II collagen degradation and its regulation in articular cartilage in osteoarthritis. Annals of the Rheumatic Diseases. 2002 November 1 [cited 2013 February 11];61(suppl 2):ii78–ii81.

43. Wu W, Billinghurst RC, Pidoux I, Antoniou J, Zukor D, Tanzer M, Poole AR. Sites of collagenase cleavage and denaturation of type II collagen in aging and osteoarthritic articular cartilage and their relationship to the distribution of matrix metalloproteinase 1 and matrix metalloproteinase 13. Arthritis and rheumatism. 2002 August;46(8):2087–2094.

44. Lippiello L, Hall D, Mankin HJ. Collagen synthesis in normal and osteoarthritic human cartilage. The Journal of clinical investigation. 1977 April;59(4):593–600.

45. Hollander AP, Pidoux I, Reiner A, Rorabeck C, Bourne R, Poole AR. Damage to type II collagen in aging and osteoarthritis starts at the articular surface, originates around chondrocytes, and extends into the cartilage with progressive degeneration. The Journal of clinical investigation. 1995 December;96(6):2859–2869.

46. Nieminen MT, Rieppo J, Töyräs J, Hakumäki JM, Silvennoinen J, Hyttinen MM, Helminen HJ, Jurvelin JS. T2 relaxation reveals spatial collagen architecture in articular cartilage: a comparative quantitative MRI and polarized light microscopic study. Magnetic resonance in medicine: official journal of the Society of Magnetic Resonance in Medicine / Society of Magnetic Resonance in Medicine. 2001 September;46(3):487–493.

47. Xia Y, Moody JB, Alhadlaq H. Orientational dependence of T2 relaxation in articular cartilage: A microscopic MRI (microMRI) study. Magnetic resonance in medicine: official journal of the Society of Magnetic Resonance in Medicine / Society of Magnetic Resonance in Medicine. 2002 September;48(3):460–469.

48. Xia Y, Moody JB, Burton-Wurster N, Lust G. Quantitative in situ correlation between microscopic MRI and polarized light microscopy studies of articular cartilage. Osteoarthritis and cartilage / OARS, Osteoarthritis Research Society. 2001 July;9(5):393–406.

49. Alhadlaq HA, Xia Y, Moody JB, Matyas JR. Detecting structural changes in early experimental osteoarthritis of tibial cartilage by microscopic magnetic resonance imaging and polarised light microscopy. Annals of the rheumatic diseases. 2004 June;63(6):709–717.

50. Bi X, Yang X, Bostrom MPG, Bartusik D, Ramaswamy S, Fishbein KW, Spencer RG, Camacho NP. Fourier transform infrared imaging and MR microscopy studies detect compositional and structural changes in cartilage in a rabbit model of osteoarthritis. Analytical and bioanalytical chemistry. 2007 March;387(5):1601–1612.

51. Gründer W, Wagner M, Werner A. MR-microscopic visualization of anisotropic internal cartilage structures using the magic angle technique. Magnetic resonance in medicine: official

journal of the Society of Magnetic Resonance in Medicine / Society of Magnetic Resonance in Medicine. 1998 March;39(3):376–382.

52. Henkelman RM, Stanisz GJ, Graham SJ. Magnetization transfer in MRI: a review. NMR in Biomedicine. 2001 April [cited 2011 July 5];14(2):57–64.

53. Wolff SD, Balaban RS. Magnetization transfer contrast (MTC) and tissue water proton relaxation in vivo. Magnetic Resonance in Medicine: Official Journal of the Society of Magnetic Resonance in Medicine / Society of Magnetic Resonance in Medicine. 1989 April [cited 2011 July 8];10(1):135–144.

54. Yarnykh VL, Yuan C. Cross-relaxation imaging reveals detailed anatomy of white matter fiber tracts in the human brain. NeuroImage. 2004 September [cited 2011 July 5];23(1):409–424.

55. Stikov N, Keenan KE, Pauly JM, Smith RL, Dougherty RF, Gold GE. Cross-relaxation imaging of human articular cartilage. Magnetic Resonance in Medicine: Official Journal of the Society of Magnetic Resonance in Medicine / Society of Magnetic Resonance in Medicine [Internet]. 2011 March 17 [cited 2011 July 5]. Available from: http://www.ncbi.nlm.nih.gov/pubmed/21416504

56. Mossahebi P, Yarnykh VL, Samsonov A. Analysis and correction of biases in cross-relaxation MRI due to biexponential longitudinal relaxation. Magnetic resonance in medicine: official journal of the Society of Magnetic Resonance in Medicine / Society of Magnetic Resonance in Medicine. 2013 February 25.

57. Sled JG, Pike GB. Quantitative interpretation of magnetization transfer in spoiled gradient echo MRI sequences. Journal of Magnetic Resonance (San Diego, Calif.: 1997). 2000 July [cited 2011 July 5];145(1):24–36.

58. Sled JG, Pike GB. Quantitative imaging of magnetization transfer exchange and relaxation properties in vivo using MRI. Magnetic resonance in medicine: official journal of the Society of Magnetic Resonance in Medicine / Society of Magnetic Resonance in Medicine. 2001 November;46(5):923–931.

59. Ramani A, Dalton C, Miller DH, Tofts PS, Barker GJ. Precise estimate of fundamental in-vivo MT parameters in human brain in clinically feasible times. Magnetic resonance imaging. 2002 December;20(10):721–731.

60. Tozer D, Ramani A, Barker GJ, Davies GR, Miller DH, Tofts PS. Quantitative magnetization transfer mapping of bound protons in multiple sclerosis. Magnetic resonance in medicine: official journal of the Society of Magnetic Resonance in Medicine / Society of Magnetic Resonance in Medicine. 2003 July;50(1):83–91.

61. Portnoy S, Stanisz GJ. Modeling pulsed magnetization transfer. Magnetic resonance in medicine: official journal of the Society of Magnetic Resonance in Medicine / Society of Magnetic Resonance in Medicine. 2007 July;58(1):144–155.

62. Yarnykh VL. Actual flip-angle imaging in the pulsed steady state: a method for rapid three-dimensional mapping of the transmitted radiofrequency field. Magnetic Resonance in Medicine: Official Journal of the Society of Magnetic Resonance in Medicine / Society of Magnetic Resonance in Medicine. 2007 January [cited 2011 July 6];57(1):192–200.

63. Deoni SCL, Rutt BK, Peters TM. Rapid combined T1 and T2 mapping using gradient recalled acquisition in the steady state. Magnetic Resonance in Medicine: Official Journal of the Society of Magnetic Resonance in Medicine / Society of Magnetic Resonance in Medicine. 2003 March [cited 2011 July 6];49(3):515–526.

64. Walter F. Block. Effects of Undersampling Errors in qMT Imaging:_ How Can It Guide Compressed Sensing Strategies for Joint Imaging? Proceedings from ISMRM Data Sampling & Image Reconstruction Workshop in Sedona, AZ. 2013.

65. Edzes HT, Samulski ET. Cross relaxation and spin diffusion in the proton NMR or hydrated collagen. Nature. 1977 February 10;265(5594):521–523.

66. Yarnykh VL. Fast macromolecular proton fraction mapping from a single off-resonance magnetization transfer measurement. Magnetic resonance in medicine: official journal of the Society of Magnetic Resonance in Medicine / Society of Magnetic Resonance in Medicine. 2012 July;68(1):166–178.

67. Helms G, Hagberg GE. In vivo quantification of the bound pool T1 in human white matter using the binary spin-bath model of progressive magnetization transfer saturation. Physics in medicine and biology. 2009 December 7;54(23):N529–540.

68. Kijowski R. Quantitative Magnetization Transfer Imaging of Human Patellar Cartilage. 39th Annual Meeting of International Skeletal Society, Rome, Italy. 2012.

69. Levesque IR, Sled JG, Pike GB. Iterative optimization method for design of quantitative magnetization transfer imaging experiments. Magnetic resonance in medicine: official journal of the Society of Magnetic Resonance in Medicine / Society of Magnetic Resonance in Medicine. 2011 September;66(3):635–643.

70. Altman R, Asch E, Bloch D, Bole G, Borenstein D, Brandt K, Christy W, Cooke TD, Greenwald R, Hochberg M. Development of criteria for the classification and reporting of osteoarthritis. Classification of osteoarthritis of the knee. Diagnostic and Therapeutic Criteria Committee of the American Rheumatism Association. Arthritis and rheumatism. 1986 August;29(8):1039–1049.

71. Felson DT, McAlindon TE, Anderson JJ, Naimark A, Weissman BW, Aliabadi P, Evans S, Levy D, LaValley MP. Defining radiographic osteoarthritis for the whole knee. Osteoarthritis and cartilage / OARS, Osteoarthritis Research Society. 1997 July;5(4):241–250.

72. Altman RD, Hochberg M, Murphy WA Jr, Wolfe F, Lequesne M. Atlas of individual radiographic features in osteoarthritis. Osteoarthritis and cartilage / OARS, Osteoarthritis Research Society. 1995 September;3 Suppl A:3–70.

73. Reeder SB, McKenzie CA, Pineda AR, Yu H, Shimakawa A, Brau AC, Hargreaves BA, Gold GE, Brittain JH. Water-fat separation with IDEAL gradient-echo imaging. Journal of magnetic resonance imaging: JMRI. 2007 March;25(3):644–652.

74. Laurent D, Wasvary J, Yin J, Rudin M, Pellas TC, O'Byrne E. Quantitative and qualitative assessment of articular cartilage in the goat knee with magnetization transfer imaging. Magnetic Resonance Imaging. 2001 December [cited 2011 July 5];19(10):1279–1286.

75. Hunter DJ, Lo GH, Gale D, Grainger AJ, Guermazi A, Conaghan PG. The reliability of a new scoring system for knee osteoarthritis MRI and the validity of bone marrow lesion assessment: BLOKS (Boston Leeds Osteoarthritis Knee Score). Annals of the rheumatic diseases. 2008 February;67(2):206–211.

76. Velikina JV, Alexander AL, Samsonov A. Accelerating MR parameter mapping using sparsity-promoting regularization in parametric dimension. Magnetic resonance in medicine: official journal of the Society of Magnetic Resonance in Medicine / Society of Magnetic Resonance in Medicine. 2012 December 4.

77. Dietrich O, Raya JG, Reeder SB, Reiser MF, Schoenberg SO. Measurement of signal-to-noise ratios in MR images: influence of multichannel coils, parallel imaging, and reconstruction filters. Journal of magnetic resonance imaging: JMRI. 2007 August;26(2):375–385.

78. Yao W, Qu N, Lu Z, Yang S. The application of T1 and T2 relaxation time and magnetization transfer ratios to the early diagnosis of patellar cartilage osteoarthritis. Skeletal radiology. 2009 November;38(11):1055–1062.

79. Mossahebi P, Chaudhary R, Sritanyaratana N, Samsonov A, Block WF, Kijowski R. Factors Influencing Quantitative Magnetization Transfer (qMT) Parameters of Articular Cartilage. 2013.

80. Lin P-C, Reiter DA, Spencer RG. Sensitivity and specificity of univariate MRI analysis of experimentally degraded cartilage. Magnetic resonance in medicine: official journal of the Society of Magnetic Resonance in Medicine / Society of Magnetic Resonance in Medicine. 2009 November;62(5):1311–1318.

81. Torchia DA, Hasson MA, Hascall VC. Investigation of molecular motion of proteoglycans in cartilage by 13C magnetic resonance. The Journal of biological chemistry. 1977 June 10;252(11):3617–3625.

82. Multanen J, Rauvala E, Lammentausta E, Ojala R, Kiviranta I, Häkkinen A, Nieminen MT, Heinonen A. Reproducibility of imaging human knee cartilage by delayed gadolinium-enhanced MRI of cartilage (dGEMRIC) at 1.5 Tesla. Osteoarthritis and cartilage / OARS, Osteoarthritis Research Society. 2009 May;17(5):559–564.

83. Glaser C, Mendlik T, Dinges J, Weber J, Stahl R, Trumm C, Reiser M. Global and regional reproducibility of T2 relaxation time measurements in human patellar cartilage. Magnetic resonance in medicine: official journal of the Society of Magnetic Resonance in Medicine / Society of Magnetic Resonance in Medicine. 2006 September;56(3):527–534.

84. Mosher TJ, Zhang Z, Reddy R, Boudhar S, Milestone BN, Morrison WB, Kwoh CK, Eckstein F, Witschey WRT, Borthakur A. Knee articular cartilage damage in osteoarthritis: analysis of MR image biomarker reproducibility in ACRIN-PA 4001 multicenter trial. Radiology. 2011 March;258(3):832–842.

85. Sritanyaratana N. Optimizing MT Point Selections for Knee qMT as a First Step in Evaluating the Tibiofemoral Joint. Proceedings from 21st Annual Meeting of ISMRM, Salt Lake City, USA. 2013.

86. Cercignani M, Alexander DC. Optimal acquisition schemes for in vivo quantitative magnetization transfer MRI. Magnetic resonance in medicine: official journal of the Society of Magnetic Resonance in Medicine / Society of Magnetic Resonance in Medicine. 2006 October;56(4):803–810.

87. Sritanyaratana N, Samsonov A, Al Saleh HA, Johnson KM, Block WF, Kijowski R. Quantitative Magnetization Transfer Analysis of In-Vivo Human Patellar Cartilage at 3.0T. Proceedings from 20th Annual Meeting of ISMRM, Melbourne, Australia. 2012.

88. Sritanyaratana N, Samsonov AA, Hurley SA, Johnson KM, Mossahebi P, Block WF, Kijowski R. Quantitative Magnetization Transfer of Entire Human Patellofemoral Joint in 30 Minutes. Proceedings from 19th Annual Meeting of ISMRM, Montreal, Canada. 2011.

89. Chen J-H, Le HC, Koutcher JA, Singer S. Fat-free MRI based on magnetization exchange. Magnetic resonance in medicine: official journal of the Society of Magnetic Resonance in Medicine / Society of Magnetic Resonance in Medicine. 2010 March;63(3):713–718.

90. Cong Z, Samsonov AA, Mossahebi P, Sritanyaratana N, Kijowski R, Block WF. Rapid Fat/Water Segmentation Using Absence of a Magnetization Transfer Effect in Fat. ISMRM Scientific Workshop on Fat-Water Separation at Long Beach, CA. 2012.

91. Bube KP, Langan RT. Hybrid minimization with applications to tomography. GEOPHYSICS. 1997 July [cited 2014 April 18];62(4):1183–1195.